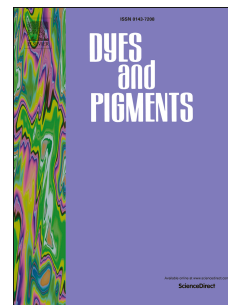


# Journal Pre-proof

Synthesis, electronic structure, linear and nonlinear photophysical properties of novel asymmetric branched compounds

Zhi-Bin Cai, Li-Jun Chen, Sheng-Li Li, Qing Ye, Yu-Peng Tian



PII: S0143-7208(19)31941-2

DOI: <https://doi.org/10.1016/j.dyepig.2019.108115>

Reference: DYPI 108115

To appear in: *Dyes and Pigments*

Received Date: 16 August 2019

Revised Date: 6 December 2019

Accepted Date: 6 December 2019

Please cite this article as: Cai Z-B, Chen L-J, Li S-L, Ye Q, Tian Y-P, Synthesis, electronic structure, linear and nonlinear photophysical properties of novel asymmetric branched compounds, *Dyes and Pigments* (2020), doi: <https://doi.org/10.1016/j.dyepig.2019.108115>.

This is a PDF file of an article that has undergone enhancements after acceptance, such as the addition of a cover page and metadata, and formatting for readability, but it is not yet the definitive version of record. This version will undergo additional copyediting, typesetting and review before it is published in its final form, but we are providing this version to give early visibility of the article. Please note that, during the production process, errors may be discovered which could affect the content, and all legal disclaimers that apply to the journal pertain.

© 2019 Published by Elsevier Ltd.

# Synthesis, electronic structure, linear and nonlinear photophysical properties of novel asymmetric branched compounds

Zhi-Bin Cai<sup>a,\*</sup>, Li-Jun Chen<sup>a</sup>, Sheng-Li Li<sup>b</sup>, Qing Ye<sup>a</sup>, Yu-Peng Tian<sup>b</sup>

<sup>a</sup> College of Chemical Engineering, Zhejiang University of Technology, Hangzhou 310014, P. R. China

<sup>b</sup> Department of Chemistry, Anhui Province Key Laboratory of Functional Inorganic Materials, Anhui University, Hefei 230039, P. R. China

\* Corresponding author.

E-mail address: caizbmail@126.com (Z.-B. Cai).

**Abstract:** A series of novel asymmetric branched compounds that utilize a 1,3,5-triazine core and feature D- $\pi$ -A-( $\pi$ -D'- $\pi$ -A')<sub>0-2</sub> configurations (D = donor, A = acceptor,  $\pi$  = conjugated bridge) were designed, successfully synthesized, and fully characterized by <sup>1</sup>H NMR, <sup>13</sup>C NMR, FT-IR, and HRMS. Their photophysical properties including linear absorption, one-photon excited fluorescence, two-photon absorption, and frequency up-converted fluorescence, were systematically investigated in different solvents. With a rise in the polarity of solvents, the peak positions of the one-photon excited fluorescence are red-shifted and the Stokes shifts increase, while the linear absorption wavelengths change slightly. In addition, the target compounds except **CZ** show the positive solvatokinetic effect. With a rise in the number of branches, the red shifts of the absorption and emission maxima, the hyperchromicity of the molar absorption coefficients, and the decrease of the Stokes shifts are observed. The peripheral electron donors (carbazole, phenothiazine) and

acceptors (pyridine, benzimidazole) also exert an important influence on the photophysical properties. Under excitation of 690-930 nm femtosecond laser pulses, all the target compounds emit frequency up-converted fluorescence with the maximal peaks at 471-575 nm, and the two-photon absorption cross-sections in THF are 132 (**PTZ**), 182 (**CZ**), 453 (**CZ-Py1**), 844 (**CZ-Py2**), 1244 (**CZ-BI1**), and 2072 (**CZ-BI2**) GM, respectively. Their two-photon response is found to be nearly additive with respect to the number of branches. The time-dependent density functional theory calculations were conducted to gain an insight into their electronic structures and to better understand the structure-photophysical property relationships. The results clearly indicate the importance of appropriate structural units on the enhancement of two-photon absorption properties.

**Keywords:** two-photon absorption, fluorescence, asymmetric branched compound, structure-property relationship

## 1. Introduction

Two-photon absorption (TPA) is a nonlinear optical phenomenon that involves the excitation of a molecule by simultaneous absorption of two photons [1]. TPA materials are of great interest in current research due to their many potential applications such as optical power limiting [2], two-photon pumped up-converted lasing [3], two-photon fluorescence imaging [4], three-dimensional optical data storage [5], three-dimensional microfabrication [6], and two-photon dynamic therapy [7].

The TPA cross-section ( $\sigma$ ) is the most important parameter used to evaluate TPA properties of materials. Therefore, to realize the above-mentioned applications, great efforts have been focused on the design and synthesis of novel materials with large  $\sigma$ . Many studies reveal that  $\sigma$  can substantially increase by incorporating several dipolar

or quadrupolar chromophores into one molecular structure through a common core, in which multi-branched architectures produce the cooperative enhancement effect. For example, Zhao *et al.* [8] synthesized novel multi-branched TPA dyes containing ketocoumarin, the largest  $\sigma$  was obtained to be 1117 GM. He *et al.* [9] synthesized a new series of linear and multi-branched bithiazole-based compounds possessing terminal triphenylamine groups, the  $\sigma$  values of the multi-branched compounds (1132 and 1665 GM) increase obviously compared with those of the linear counterparts (173 and 429 GM). Thus, multi-branched architectures have become an effective strategy in the molecular design of TPA materials.

Multi-branched architectures greatly extend the molecular  $\pi$ -conjugated systems. A high degree of electron delocalization in the whole  $\pi$ -system is considered to be the key factor to improve  $\sigma$ . So in the design of multi-branched TPA materials, it is important to select appropriate cores, peripheral moieties, and branch configurations which can facilitate intramolecular charge transfer (ICT). Recently, many heterocycle-based TPA materials with large  $\sigma$  have been reported [10]. It was found that  $\pi$ -deficient and  $\pi$ -excessive heterocycles may act as efficient electron acceptors (A) and donors (D), respectively. Additionally, molecules based on heterocycle(s) often emit strong fluorescence, which is an important prerequisite for some TPA-based applications such as fluorescence microscopy. 1,3,5-Triazine is a heterocycle, analogous to the six-membered benzene ring but with three alternate carbon atoms replaced by nitrogen atoms. It is more  $\pi$ -electron-deficient than other heterocyclic rings and thus can be used as an effective electron acceptor. In addition, the structural symmetry and the spatial coplanarity make it easier to become a core which can be functionalized with a variety of desired molecules. For example, Wang *et al.* [11] investigated several modified triple-branched compounds based on a 1,3,5-triazine core, the results indicate that these compounds exhibit good TPA and two-photon fluorescence properties. Yang *et al.* [12] synthesized a diketopyrrolopyrrole-based multi-branched derivative with a 1,3,5-triazine core, which exhibits good TPA and aggregation-induced emission properties. The aromatic heterocycle carbazole has perfect coplanarity and its electron density is much richer

compared with benzene and fluorene, for a lone pair of electrons on the nitrogen atom participates in forming its large  $\pi$ -bond [13]. Phenothiazine is a recognized pharmaceutical molecule bearing electron-rich nitrogen and sulfur heteroatoms, and its ring is nonplanar with a butterfly conformation in the ground state, which can impede the molecular aggregation and the formation of intermolecular excimer [14]. Both carbazole and phenothiazine can be used as efficient electron donors. Likewise, as nitrogen-containing heterocyclic molecules, pyridine and imidazole have strong electron-withdrawing ability and good coplanarity, rendering them to be ideal electron acceptors for nonlinear optical materials [15]. Up till now, the reported multi-branched TPA materials generally adopt exactly the same branches [16], while it is rarely reported that different structural units are introduced into branches or different branch configurations are combined to construct asymmetric multi-branched TPA materials [17]. Therefore, the relationship between structures and properties of multi-branched TPA materials modulated by asymmetry remains largely unclear. In addition, the multi-branched TPA materials reported so far usually adopt two branch configurations: a D- $\pi$ -A dipolar structure [18] and a D- $\pi$ -D quadrupolar structure [19]. Compared with D- $\pi$ -D quadrupolar structures, A- $\pi$ -D- $\pi$ -A quadrupolar structures introduce electron acceptors [20], large  $\sigma$  may be achieved by stronger ICT from the central donor to the peripheral acceptors through various conjugated linkages upon optical excitation. For example, Liu *et al.* [21] synthesized a D- $\pi$ -D molecule based on two triphenylamine donors and its  $\sigma$  is 75 GM. Katan *et al.* [22] synthesized a A- $\pi$ -D- $\pi$ -A molecule based on a triphenylamine center and two octylsulfonyl end groups, whose  $\sigma$  (420 GM) increases obviously.

In this work, we designed a series of novel asymmetric single-branched (**PTZ**, **CZ**), double-branched (**CZ-Py1**, **CZ-BI1**), and triple-branched (**CZ-Py2**, **CZ-BI2**) compounds built from a 1,3,5-triazine core, in which carbazole (or phenothiazine) and pyridine (or benzimidazole) were selected as the peripheral electron donor and acceptor, respectively, and the electron-donating methoxy groups were introduced in the middle of the branch as the auxiliary donors (Fig. 1). Their configurations are in the form of D- $\pi$ -A (**PTZ**, **CZ**), D- $\pi$ -A- $\pi$ -D'- $\pi$ -A' (**CZ-Py1**, **CZ-BI1**), and

$D-\pi-A-(\pi-D'-\pi-A')$ <sub>2</sub> (**CZ-Py2**, **CZ-BI2**), respectively. To our knowledge, the asymmetric multi-branched TPA materials formed by incorporating dipolar  $D-\pi-A$  and quasi-quadrupolar  $A-\pi-D-\pi-A'$  branches into a 1,3,5-triazine core have not been reported. All the target compounds were successfully synthesized and fully characterized by <sup>1</sup>H NMR, <sup>13</sup>C NMR, FT-IR, and HRMS. Their linear and nonlinear photophysical properties were systematically investigated in different solvents. The time-dependent density functional theory (TDDFT) calculations were used to complement and to rationalize experimental findings.

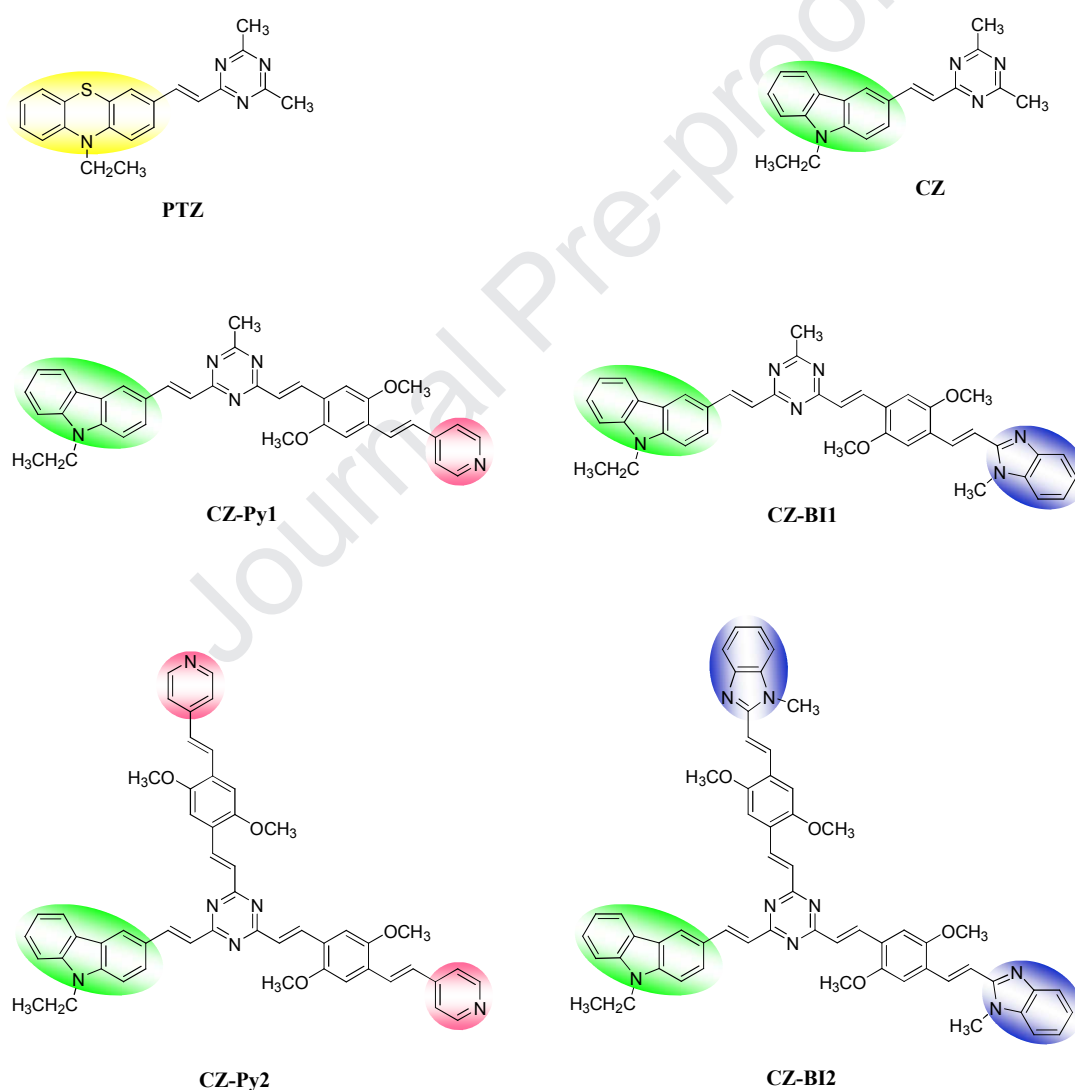


**Fig. 1.** Molecular structures of the target compounds.

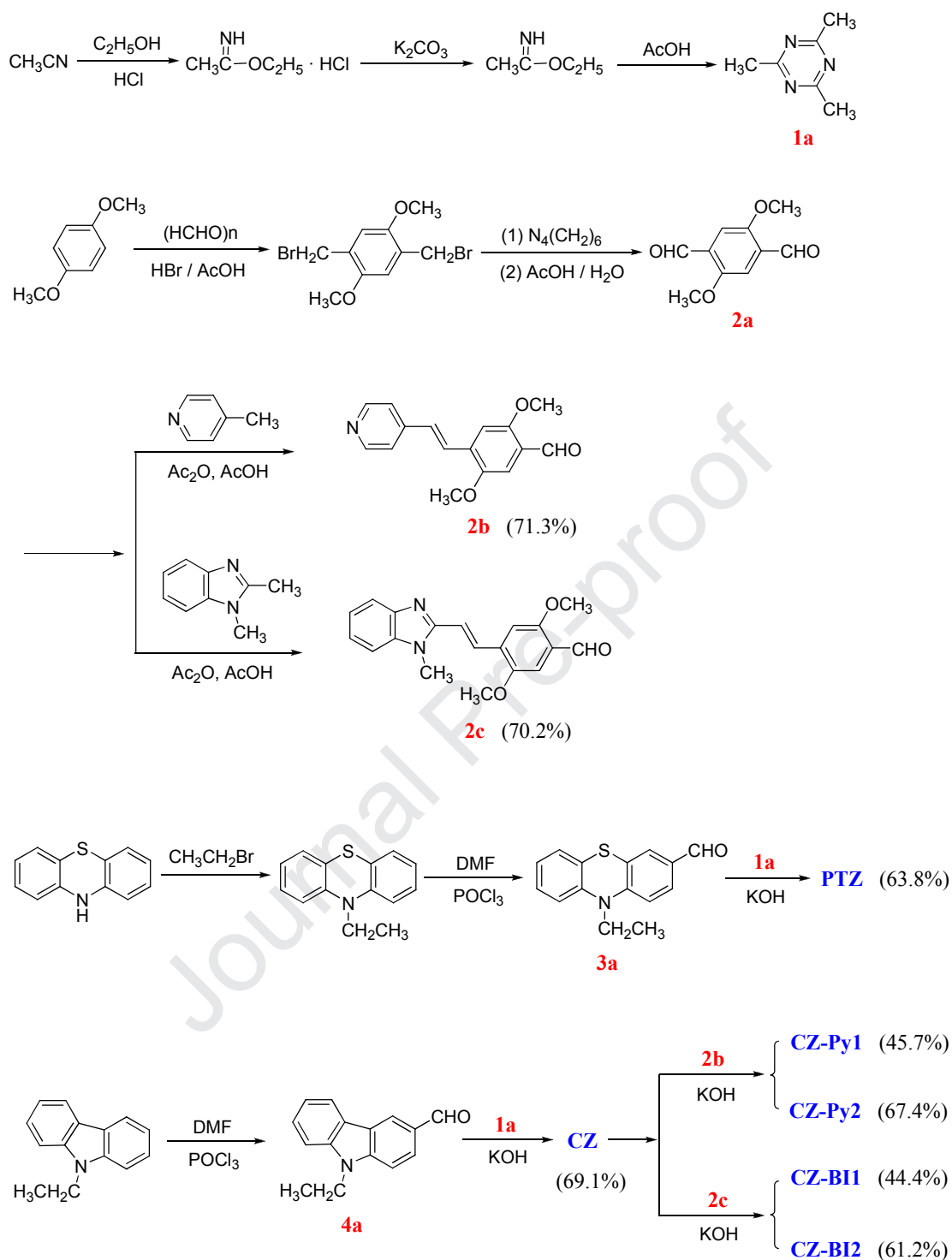
## 2. Results and discussion

### 2.1. Synthesis and characterization

The synthetic routes of the target compounds are shown in Scheme 1. 2,4,6-Trimethyl-1,3,5-triazine (**1a**) [23], 2,5-dimethoxy-1,4-benzenedicarboxaldehyde (**2a**) [24], 1,2-dimethyl-1*H*-benzimidazole [25], 10-ethyl-10*H*-phenothiazine-3-carboxaldehyde (**3a**) [26], and 9-ethyl-9*H*-carbazole-3-carboxaldehyde (**4a**) [27] were synthesized according to the literature procedures. 2,5-Dimethoxy-4-[(1*E*)-2-(4-pyridinyl)ethenyl]benzaldehyde (**2b**) [24] and 2,5-dimethoxy-4-[(1*E*)-2-(1-methyl-1*H*-benzimidazol-2-yl)ethenyl]benzaldehyde (**2c**) were prepared by the condensation of 4-methylpyridine and 1,2-dimethyl-1*H*-benzimidazole with **2a** in a solution of acetic anhydride and acetic acid, respectively. **2c** was reported here for the first time. The alkaline condensation of **1a** with the corresponding aldehydes (**3a**, **4a**) in methanol gave two new target compounds (**PTZ**, **CZ**). Then **CZ** continued to undergo alkaline condensation with **2b** or **2c** to give the other four new target compounds (**CZ-Py1**, **CZ-Py2**, **CZ-BI1**, and **CZ-BI2**) in moderate yields.

Column chromatographic purification of the target compounds was performed on silica gel (200-300 mesh). All of them were fully characterized by <sup>1</sup>H NMR, <sup>13</sup>C NMR, FT-IR, and HRMS. The <sup>1</sup>H NMR spectra show the doublets for olefinic protons at 8.49-8.57, 8.02-8.47, 7.71-8.20, 7.45-7.62, 7.37-7.43, and 7.03-7.32 ppm with the coupling constants of 15.8-16.6 Hz, which suggests the *E*-configurations. The protons in the carbazole ring exhibit seven groups of peaks: four doublets at 8.68-8.74, 8.25-8.31, 7.68-7.71, and 7.66-7.67 ppm, one double doublet at 7.93-7.98 ppm, and two triplets at 7.50-7.52 and 7.27-7.29 ppm. The protons in the pyridine ring exhibit two groups of peaks: two doublets at 8.57 and 7.56-7.57 ppm. The protons in the benzimidazole ring exhibit three groups of peaks: two double doublets at 7.64-7.65 and 7.56 ppm and one multiplet at 7.21-7.28 ppm. For the single- and double-branched compounds (**PTZ**, **CZ**, **CZ-Py1**, and **CZ-BI1**), the singlets at

2.53-2.63 ppm are attributed to the protons in the methyl group(s) linked to the triazine ring, which disappear completely in the triple-branched compounds (**CZ-Py2**, **CZ-BI2**). Moreover, it can be seen that the chemical shifts of the protons in the olefinic group linked to the benzimidazole ring (about 7.62 and 8.20 ppm) move to lower fields compared with those linked to the pyridine ring (about 7.45 and 7.71 ppm). This indicates that benzimidazole has stronger electron-withdrawing ability than pyridine. In the FT-IR spectra, the characteristic absorption peaks appearing at 1232-1246  $\text{cm}^{-1}$  and 1328-1346  $\text{cm}^{-1}$  are attributed to the stretching vibration of -C-N and =C-N, respectively. The peaks at 1211  $\text{cm}^{-1}$  belong to the C-O-C asymmetric stretching vibration, and those at 1040-1042  $\text{cm}^{-1}$  belong to the C-O-C symmetric stretching vibration. The skeleton vibration absorption peaks of the triazine ring appear at 1504-1530  $\text{cm}^{-1}$ , whose values decrease from 1524  $\text{cm}^{-1}$  to 1519 (1519)  $\text{cm}^{-1}$  and 1504 (1505)  $\text{cm}^{-1}$  when going from **CZ** to **CZ-Py1** (**CZ-BI1**) and **CZ-Py2** (**CZ-BI2**). The peaks at 973-980  $\text{cm}^{-1}$  correspond to the C-H out-of-plane bending vibration of the *trans* olefinic groups, which further supports the *E*-configurations.



Scheme 1. Synthetic routes of the target compounds.

## 2.2. Liner absorption and TDDFT calculations

The linear photophysical properties of the target compounds in different solvents

are listed in Table 1. Their linear absorption spectra in THF are shown in Fig. 2. As shown in Fig. 2, **PTZ** exhibits two major absorption bands, while the other target compounds (**CZ**, **CZ-Py1**, **CZ-Py2**, **CZ-BI1**, and **CZ-BI2**) show three major absorption bands. For the double- and triple-branched compounds, the bands observed at 293-298 and 325-363 nm can be attributed to the  $\pi$ - $\pi^*$  transition of the carbazole ring and styrene, respectively, the low-energy bands located at 410-433 nm originate from an ICT process. For the single-branched compounds, the absorption maxima ( $\lambda_{\max}^{\text{abs}}$ ) of **PTZ** with a phenothiazine donor appear at 310-312 nm, which are attributed to the  $\pi$ - $\pi^*$  transition of the phenothiazine ring, while the  $\lambda_{\max}^{\text{abs}}$  of **CZ** with a carbazole donor around 380 nm results from an ICT process. It can be seen from the data in Table 1 that the  $\lambda_{\max}^{\text{abs}}$  values change slightly ( $\leq 6$  nm) with an increase in the solvent polarity from toluene to DMF, which indicates that the surrounding solvent molecules have little influence on the transition energy of the target compounds. As the number of branches increases, the red shifts ( $\lambda_{\max}^{\text{abs}}$ ) accompanied by the hyperchromicity (the maximum molar absorption coefficient,  $\epsilon_{\max}$ ) are observed. For example, the  $\lambda_{\max}^{\text{abs}}$  ( $\epsilon_{\max}$ ) values in THF increase from 381 nm ( $3.64 \times 10^4 \text{ mol}^{-1} \text{ L cm}^{-1}$ ) to 410 nm ( $4.63 \times 10^4 \text{ mol}^{-1} \text{ L cm}^{-1}$ ) and 418 nm ( $16.22 \times 10^4 \text{ mol}^{-1} \text{ L cm}^{-1}$ ) when going from **CZ** to **CZ-Py1** and **CZ-Py2**. These can be due to the extended  $\pi$ -conjugated systems formed by incorporating more branches into the central triazine ring. Compared **CZ-Py1** with **CZ-BI1** and **CZ-Py2** with **CZ-BI2**, respectively, **CZ-BI1** and **CZ-BI2** have stronger light-absorbing ability and their transition energy between the ground and excited electronic states is lower than that of **CZ-Py1** and **CZ-Py2**.

**Table 1**

Linear photophysical properties of the target compounds.

| Compound      | Solvent                         | $\lambda_{\max}^{\text{abs}}$ <sup>a</sup><br>(nm) | $10^{-4} \epsilon$ <sup>b</sup><br>(mol <sup>-1</sup> L cm <sup>-1</sup> ) | $\lambda_{\max}^{\text{OPEF}}$ <sup>c</sup><br>(nm) | $\Delta\nu$ <sup>d</sup><br>(cm <sup>-1</sup> ) | $\Phi$ <sup>e</sup> |
|---------------|---------------------------------|--|--|---|---|---------------------|
| <b>PTZ</b>    | Toluene                         | 310  | 2.08   | 550   | 14076   | 0.31                |
|               | THF                             | 311  | 2.49   | 564   | 14424   | 0.21                |
|               | CH <sub>2</sub> Cl <sub>2</sub> | 312  | 2.70   | 583   | 14899   | 0.05                |
|               | DMF                             | 312  | 2.51   | 594   | 15216   | 0.02                |
| <b>CZ</b>     | Toluene                         | 379  | 2.65   | 435   | 3397  | 0.04                |
|               | THF                             | 381  | 3.64   | 458   | 4413  | 0.06                |
|               | CH <sub>2</sub> Cl <sub>2</sub> | 381  | 4.05   | 469   | 4925  | 0.13                |
|               | DMF                             | 383  | 3.13   | 481   | 5320  | 0.27                |
| <b>CZ-Py1</b> | Toluene                         | 410  | 4.94   | 472   | 3204  | 0.49                |
|               | THF                             | 410  | 4.63   | 485   | 3772  | 0.35                |
|               | CH <sub>2</sub> Cl <sub>2</sub> | 412  | 4.88   | 491   | 3905  | 0.24                |
|               | DMF                             | 416  | 4.14   | 500   | 4038  | 0.01                |
| <b>CZ-Py2</b> | Toluene                         | 419  | 13.43  | 479   | 2990  | 0.37                |
|               | THF                             | 418  | 16.22  | 491   | 3557  | 0.23                |
|               | CH <sub>2</sub> Cl <sub>2</sub> | 421  | 15.88  | 499   | 3713  | 0.08                |
|               | DMF                             | 424  | 14.34  | 509   | 3939  | 0.005               |
| <b>CZ-BI1</b> | Toluene                         | 421  | 6.92   | 482   | 3006  | 0.58                |
|               | THF                             | 424  | 5.12   | 499   | 3545  | 0.47                |
|               | CH <sub>2</sub> Cl <sub>2</sub> | 424  | 5.09   | 503   | 3704  | 0.39                |
|               | DMF                             | 427  | 6.64   | 512   | 3888  | 0.02                |
| <b>CZ-BI2</b> | Toluene                         | 427  | 14.34  | 485   | 2801  | 0.45                |
|               | THF                             | 429  | 17.24  | 504   | 3469  | 0.30                |
|               | CH <sub>2</sub> Cl <sub>2</sub> | 431  | 19.28  | 509   | 3555  | 0.14                |
|               | DMF                             | 433  | 20.45  | 519   | 3827  | 0.006               |

<sup>a</sup> Maximum linear absorption wavelength,  $c = 1 \times 10^{-5}$  mol L<sup>-1</sup>.

<sup>b</sup> Maximum molar absorption coefficient.

<sup>c</sup> Maximum one-photon excited fluorescence wavelength,  $c = 1 \times 10^{-6}$  mol L<sup>-1</sup>.

<sup>d</sup> Stokes shift.

<sup>e</sup> Fluorescence quantum yield.

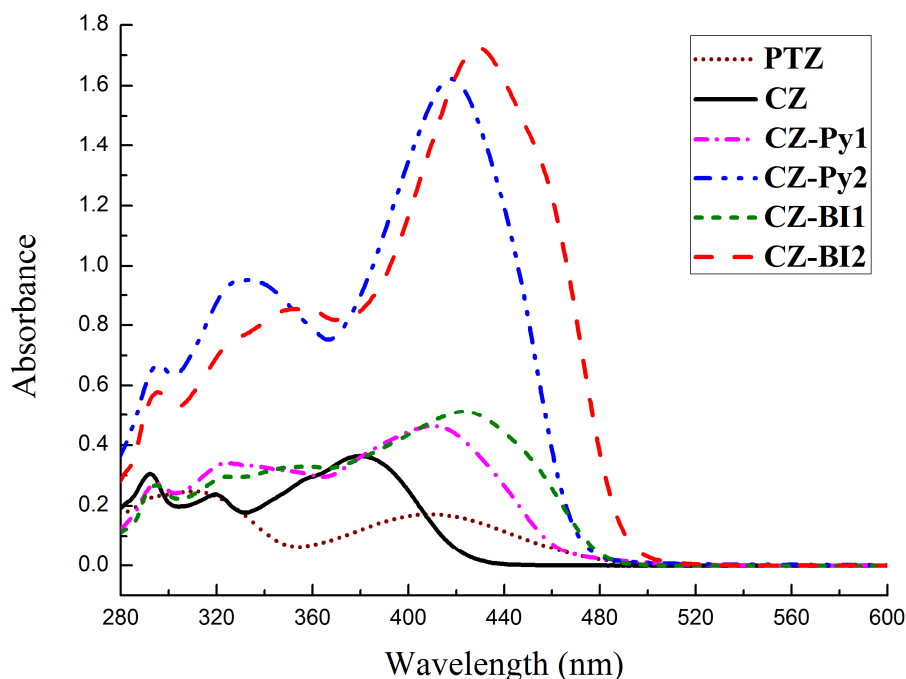


**Fig. 2.** Linear absorption spectra of the target compounds in THF ( $c = 1 \times 10^{-5}$  mol L<sup>-1</sup>).

To further rationalize the absorption spectra, the TDDFT calculations were performed using the Gaussian 09 program for the target compounds. The non-local density function of B3LYP with 6-31G (d) basis sets was used for the calculations. The ground state geometries of the target compounds were fully optimized. Table 2 suggests that the calculated  $\lambda_{\max}^{\text{abs}}$  values are in consistent with the experimental ones. The absorption peaks with the strongest oscillator strength are at 325 (**PTZ**), 373 (**CZ**), 440 (**CZ-Py1**), 452 (**CZ-Py2**), 456 (**CZ-BI1**), and 477 (**CZ-BI2**) nm,

respectively, which are primarily due to the transition from the HOMO to the LUMO (percent contributions: 81.4%-96.5%) except **PTZ** (HOMO-1→LUMO, 66.7%). The molecular orbital energy levels mainly involved are plotted, as shown in Fig. 3. The calculated HOMO-LUMO energy gaps ( $\Delta E$ ) are 3.616 (**CZ**), 3.148 (**CZ-Py1**), 3.067 (**CZ-Py2**), 2.978 (**CZ-BI1**), and 2.934 (**CZ-BI2**) eV, respectively, corresponding with the sequence of  $\lambda_{\max}^{\text{abs}}$  (**CZ** < **CZ-Py1** < **CZ-Py2** < **CZ-BI1** < **CZ-BI2**). The molecular orbits mainly involved are illustrated in Fig. 4. It can be seen clearly that the electronic transition of all the target compounds is accompanied by significant charge transfer. For **PTZ**, **CZ**, **CZ-Py1**, and **CZ-Py2**, the electron clouds of the HOMOs are distributed on the electron donors (phenothiazine, carbazole, and methoxy) and  $\pi$ -conjugated bridges (1,2-vinylene and 1,4-phenylenedivinylene), whereas in the LUMOs, most or all of the electron clouds on the above-mentioned donors have transferred to the electron acceptors (triazine and pyridine). For **CZ-BI1** and **CZ-BI2**, it is notable that the electron clouds of the HOMOs are not spread over the D- $\pi$ -A branch, but are essentially concentrated on the methoxy donor, the benzimidazole acceptor, and the 1,4-phenylenedivinylene  $\pi$ -bridge of the A- $\pi$ -D'- $\pi$ -A' branch. In the LUMOs, the electron cloud density localized on methoxy and benzimidazole decreases, while that on the strong electron-withdrawing triazine core increases obviously.

**Table 2**

Calculated and experimental absorption maxima, oscillator strength, and major orbital contributions for the target compounds.

| Compound   | Transition            | Calculated                         | Experimental                       | Oscillator strength, $f$ | Major orbital contribution                  |
|------------|-----------------------|------------------------------------|------------------------------------|--------------------------|---|
|            |                       | $\lambda_{\max}^{\text{abs}}$ (nm) | $\lambda_{\max}^{\text{abs}}$ (nm) |                          |   |
| <b>PTZ</b> | $S_0 \rightarrow S_3$ | 325                                | 310-312 <sup>a</sup>               | 0.6386                   | HOMO-1→LUMO (66.7%),<br>HOMO→LUMO+2 (20.4%) |
| <b>CZ</b>  | $S_0 \rightarrow S_1$ | 373                                | 379-383 <sup>a</sup>               | 0.7346                   | HOMO→LUMO (96.5%)                           |

|               |                       |     |                      |        |   |
|---------------|-----------------------|-----|----------------------|--------|---|
| <b>CZ-Py1</b> | $S_0 \rightarrow S_1$ | 440 | 410-416 <sup>a</sup> | 0.9124 | HOMO $\rightarrow$ LUMO (95.4%)                                       |
| <b>CZ-Py2</b> | $S_0 \rightarrow S_2$ | 452 | 418-424 <sup>a</sup> | 1.0468 | HOMO $\rightarrow$ LUMO (83.2%),<br>HOMO-1 $\rightarrow$ LUMO (9.7%)  |
| <b>CZ-BI1</b> | $S_0 \rightarrow S_1$ | 456 | 421-427 <sup>a</sup> | 1.7891 | HOMO $\rightarrow$ LUMO (90.5%)                                       |
| <b>CZ-BI2</b> | $S_0 \rightarrow S_1$ | 477 | 427-433 <sup>a</sup> | 1.8904 | HOMO $\rightarrow$ LUMO (81.4%),<br>HOMO-1 $\rightarrow$ LUMO (14.8%) |

<sup>a</sup> Data from the linear absorption spectra in different solvents.

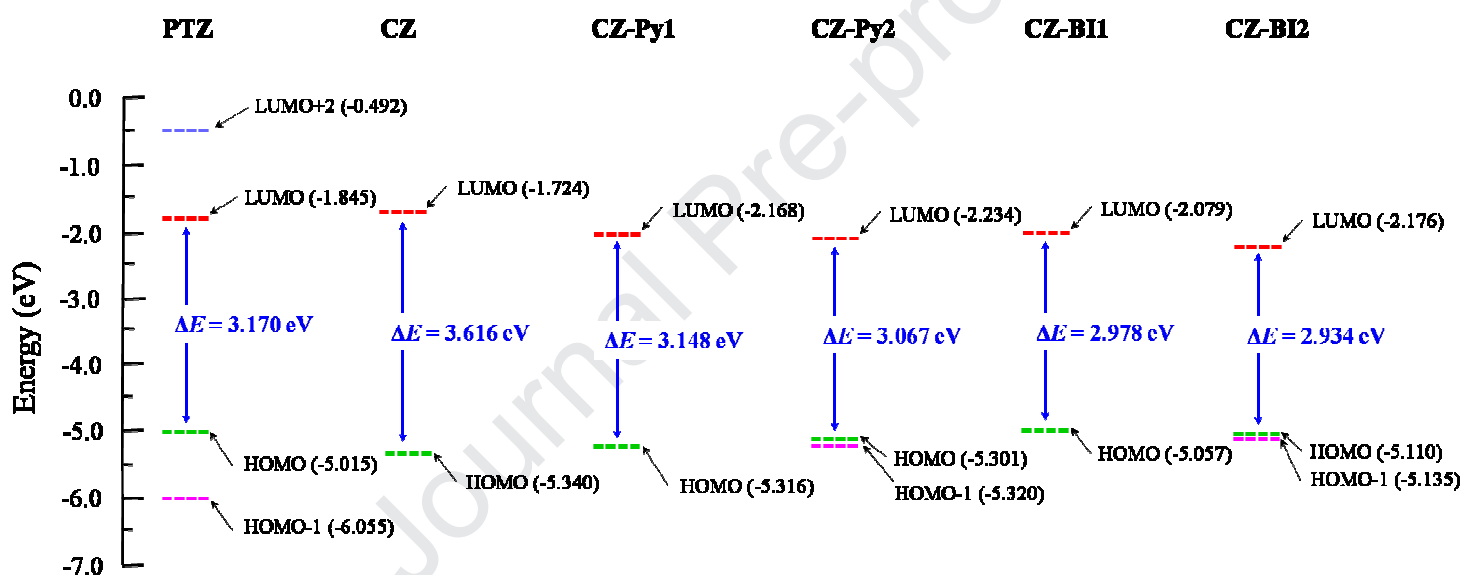


**Fig. 3.** Molecular orbital energy levels of the target compounds mainly involved in the TDDFT calculations.

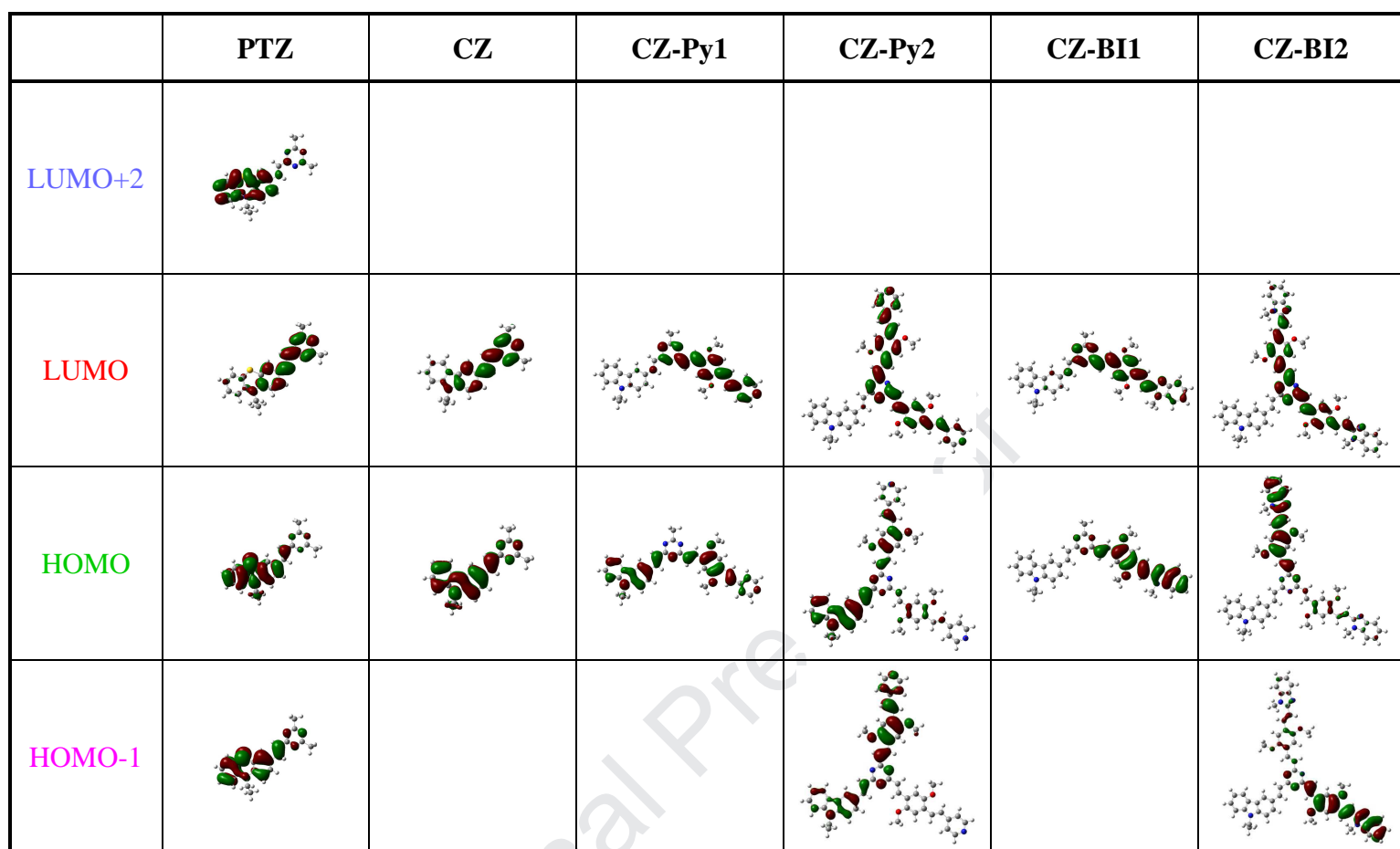
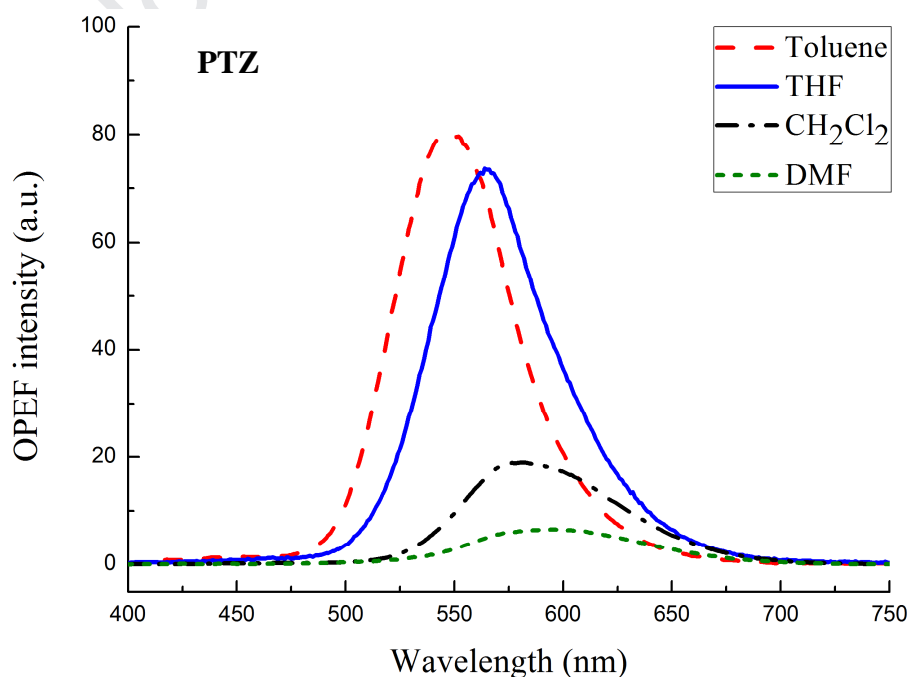


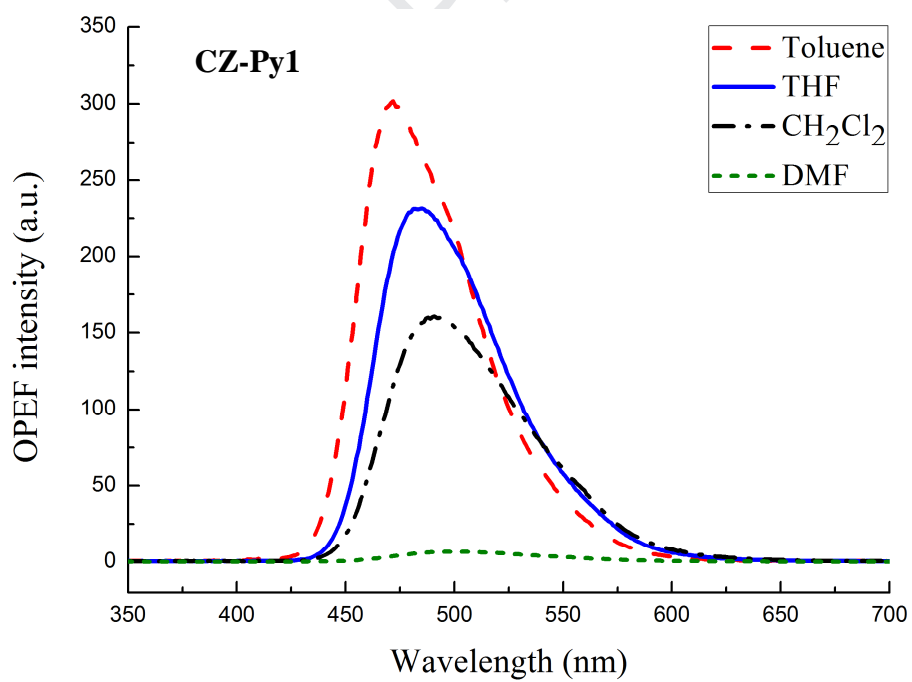
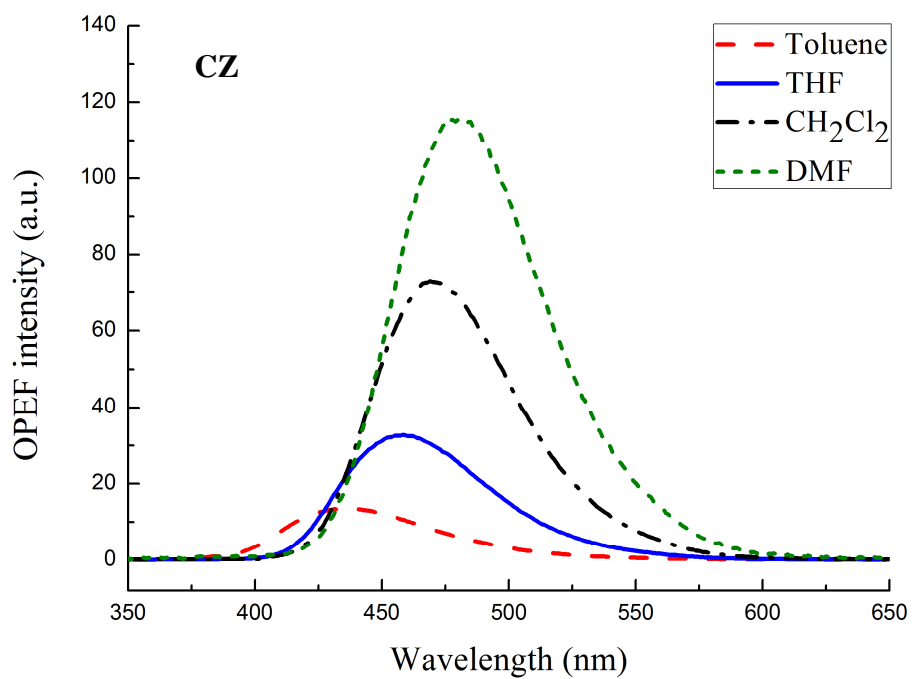
**Fig. 4.** Molecular orbitals of the target compounds mainly involved in the TDDFT calculations.

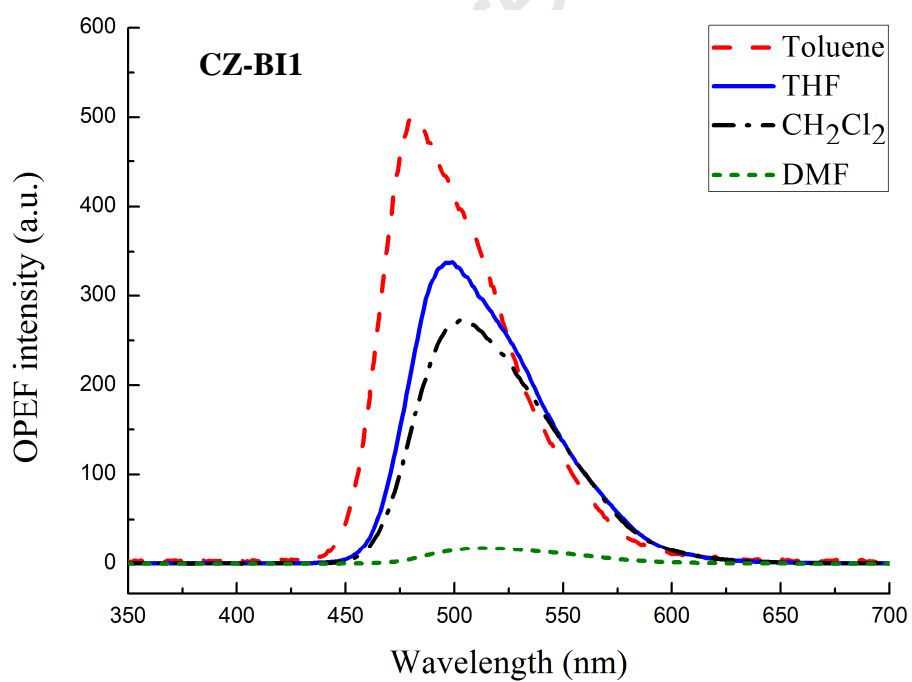
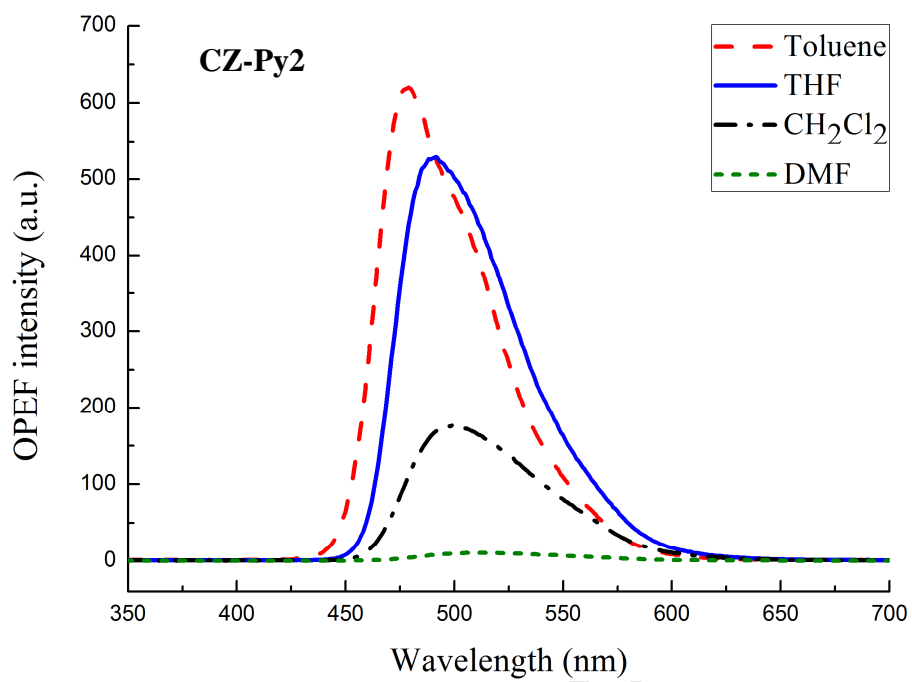
### 2.3. One-photon excited fluorescence

The one-photon excited fluorescence (OPEF) spectra of the target compounds are shown in Figs. 5 and 6. The corresponding data are listed in Table 1. Upon photoexcitation, all the target compounds exhibit a fluorescence peak located within the range from 435 to 594 nm, which can be assigned to the ICT emission. It is noticeable that the effect of solvent polarity on the emission behavior is much more pronounced than that on the absorption behavior. The empirical parameter  $E_T(30)$  has been used fairly effectively to describe solvent polarity, whose values of toluene, THF,  $\text{CH}_2\text{Cl}_2$ , and DMF are 33.9, 37.4, 40.7, and 43.2, respectively [28]. As the solvent polarity increases, the OPEF maxima ( $\lambda_{\text{max}}^{\text{OPEF}}$ ) show positive solvatochromic behavior. From toluene to DMF, the  $\lambda_{\text{max}}^{\text{OPEF}}$  values range from 550 to 594 nm for **PTZ**, from 435 to 481 nm for **CZ**, from 472 to 500 nm for **CZ-Py1**, from 479 to 509 nm for **CZ-Py2**, from 482 to 512 nm for **CZ-BI1**, and from 485 to 519 nm for **CZ-BI2**. The Stokes shifts ( $\Delta\nu$ ) exhibit the same solvent polarity dependencies as the  $\lambda_{\text{max}}^{\text{OPEF}}$ . These can be explained by the fact that the excited state may possess higher polarity than the ground state, as a result, the solute-solvent interaction in the excited state is enhanced as compared with that in the ground state, which leads to a lower energy level for the excited state and finally decreases the energy gap between the ground and excited states. Similar to the  $\lambda_{\text{max}}^{\text{abs}}$ , the  $\lambda_{\text{max}}^{\text{OPEF}}$  is also red-shifted with the increase of branches owing to the large extension of  $\pi$ -systems. For example, the  $\lambda_{\text{max}}^{\text{OPEF}}$  values in THF increase from 458 nm of **CZ** to 485 (499) nm of **CZ-Py1** (**CZ-BI1**) and 491 (504) nm of **CZ-Py2** (**CZ-BI2**). However, the  $\Delta\nu$  values display a corresponding decline, which implies that the polarity of these branched compounds in the excited state can be sequenced as **CZ** > **CZ-Py1** > **CZ-Py2** and **CZ** > **CZ-BI1** > **CZ-BI2**. In addition, inspection of the  $\lambda_{\text{max}}^{\text{OPEF}}$  as well as the  $\lambda_{\text{max}}^{\text{abs}}$  reveals that the electronic structures of the double-branched compounds **CZ-Py1** and **CZ-BI1** may be more similar to those of the corresponding triple-branched compounds **CZ-Py2** and

**CZ-BI2** (3-9 nm shifts for  $\lambda_{\max}^{\text{OPEF}}$  and 5-9 nm shifts for  $\lambda_{\max}^{\text{abs}}$ ), rather than that of the single-branched compound **CZ** (19-47 nm shifts for  $\lambda_{\max}^{\text{OPEF}}$  and 29-44 nm shifts for  $\lambda_{\max}^{\text{abs}}$ ). The influence of the peripheral electron donor on the  $\lambda_{\max}^{\text{OPEF}}$  (**PTZ** *cf.* **CZ**) is more remarkable than that of the peripheral electron acceptor on the  $\lambda_{\max}^{\text{OPEF}}$  (**CZ-Py1** *cf.* **CZ-BI1** and **CZ-Py2** *cf.* **CZ-BI2**). For example, in THF, the  $\lambda_{\max}^{\text{OPEF}}$  of **PTZ** at 564 nm is red-shifted by 106 nm relative to that of **CZ** at 458 nm (phenothiazine donor *cf.* carbazole donor), while for **CZ-Py1**, **CZ-Py2**, **CZ-BI1**, and **CZ-BI2** (pyridine acceptor *cf.* benzimidazole acceptor), the differences among  $\lambda_{\max}^{\text{OPEF}}$  do not exceed 14 nm. From the fluorescence photographs in THF (Fig. 6), it is obvious that **PTZ** and **CZ** emit fluorescence of different colors varied from orange-yellow to blue, while the colors of fluorescence are all green for **CZ-Py1**, **CZ-Py2**, **CZ-BI1**, and **CZ-BI2**. These observations indicate that the radiative transition energy of **PTZ** is far lower than that of **CZ** probably due to its significant geometric reorganization and strong solvation effect in the excited state, while the radiative transition energy of **CZ-Py1**, **CZ-Py2**, **CZ-BI1**, and **CZ-BI2** is close to each other.







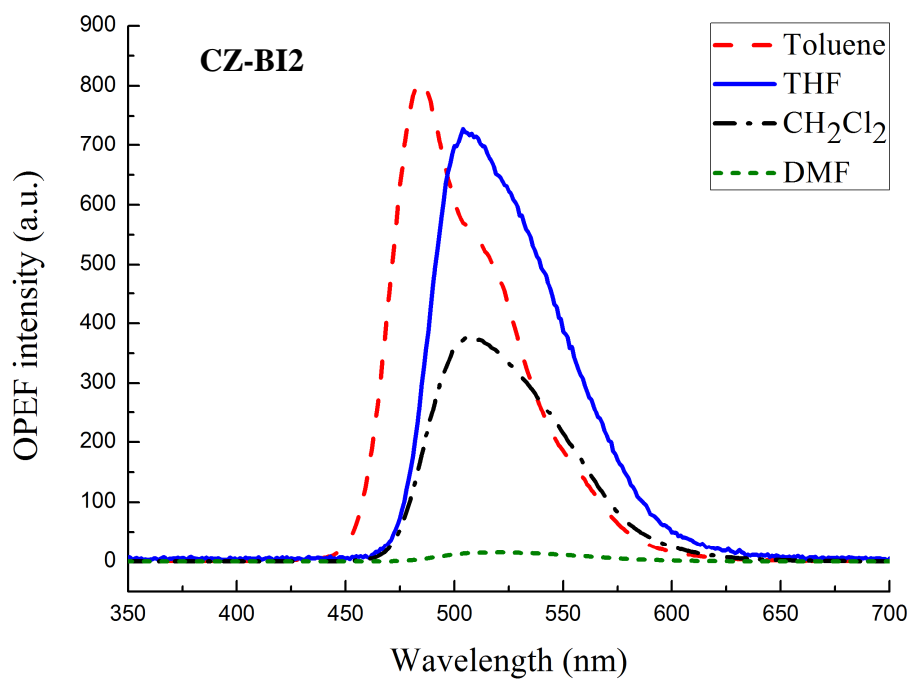


**Fig. 5.** One-photon excited fluorescence spectra of the target compounds in different solvents ( $c = 1 \times 10^{-6} \text{ mol L}^{-1}$ ).

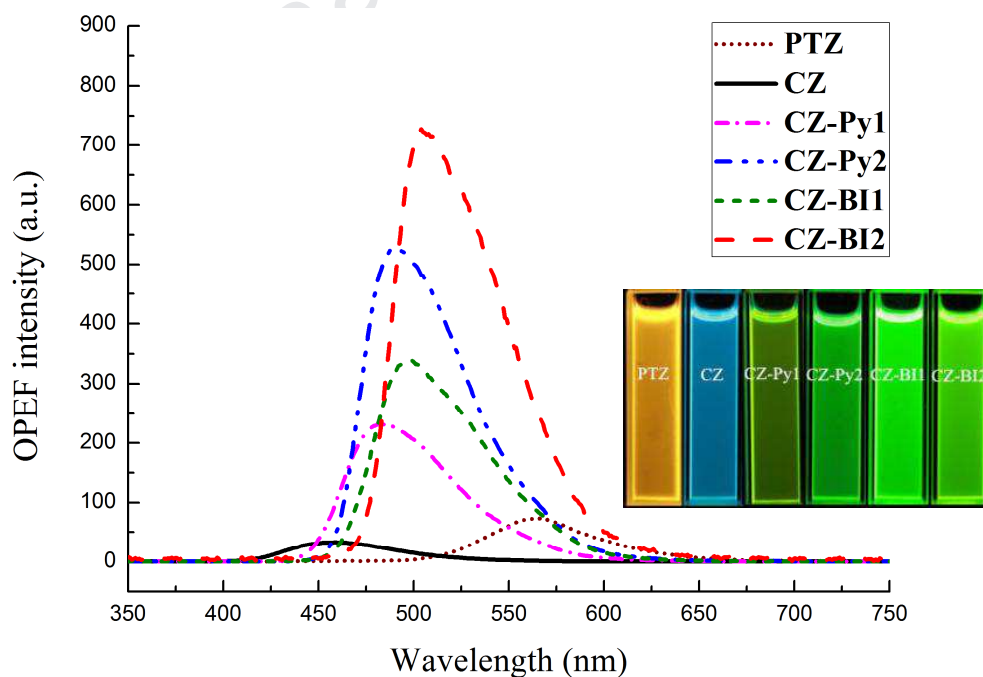


**Fig. 6.** One-photon excited fluorescence spectra and the fluorescence photographs of the target compounds in THF.

It is well accepted that the dipole moment changes are related to the optical properties of organic compounds. The Lippert-Mataga equation is widely used to estimate the dipole moment changes between the excited and ground states ( $\Delta\mu_{eg}$ ), which is as follows [29]:

$$\Delta\nu = \frac{2\Delta\mu_{eg}^2}{hca^3} \Delta f + \text{constant} \quad (1)$$

where  $\Delta\nu = \nu_{abs} - \nu_{em}$  represents the Stokes shift,  $\nu_{abs}$  ( $\nu_{em}$ ) is the wavenumber of the absorption (emission) maximum.  $\Delta\mu_{eg}$  corresponds to  $(\mu_e - \mu_g)$ ,  $\mu_e$  and  $\mu_g$  are the dipole moments of the excited and ground states, respectively.  $h$  is Planck's constant,  $c$  is the speed of light,  $a$  is the radius of the Onsager spherical cavity.  $\Delta f = (\epsilon - 1)/(2\epsilon + 1) - (n^2 - 1)/(2n^2 + 1)$  represents the orientation polarizability,  $\epsilon$  is the dielectric constant and  $n$  is the refractive index of the solvent.

The Lippert-Mataga plots for **CZ-Py1**, **CZ-Py2**, **CZ-BI1**, and **CZ-BI2** are displayed in Fig. 7. The  $\Delta\nu$  values are found to depend linearly on the orientation polarizability of the solvents ( $\Delta f$ ). The slopes ( $k$ ) derived from the fitted lines are 3172 (**CZ-Py1**), 3475 (**CZ-Py2**), 3265 (**CZ-BI1**), and 3774 (**CZ-BI2**)  $\text{cm}^{-1}$ , respectively. According to the Lippert-Mataga relationship ( $\Delta\mu_{eg}^2 = \frac{1}{2}khca^3$ ), the  $\Delta\mu_{eg}$  is proportional to the  $k$  and the Onsager radius ( $a$ ). Considering the  $k$  and the  $a$  together, the order of the  $\Delta\mu_{eg}$  should be **CZ-Py2** > **CZ-Py1**, **CZ-BI2** > **CZ-BI1**, **CZ-BI1** > **CZ-Py1**, and **CZ-BI2** > **CZ-Py2**. The increase of the  $\Delta\mu_{eg}$  is expected to result in the enhancement of TPA.

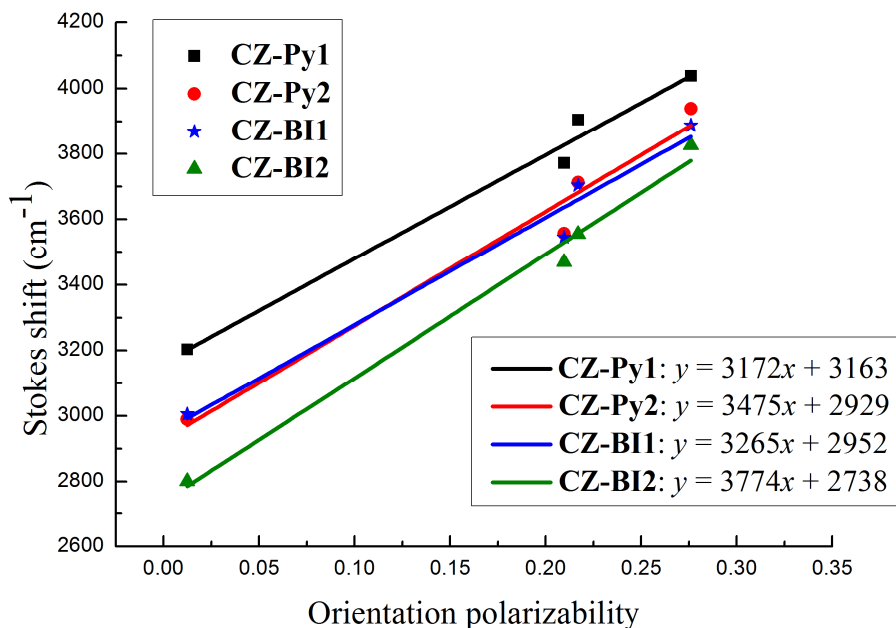


**Fig. 7.** Lippert-Mataga plots for **CZ-Py1**, **CZ-Py2**, **CZ-BI1**, and **CZ-BI2**.

The fluorescence quantum yields ( $\Phi$ ) in different solvents were calculated by Equation (2) [30]. Fluorescein in 0.1 mol L<sup>-1</sup> sodium hydroxide was used as the reference ( $\Phi = 0.9$  [30]).

$$\Phi_s = \frac{A_r n_s^2 F_s}{A_s n_r^2 F_r} \Phi_r \quad (2)$$

where the subscripts s and r denote the sample and the reference, respectively.  $A$  is the absorbance at the excitation wavelength,  $n$  is the refractive index of the relevant solution, and  $F$  is the integrated area under the corrected emission spectrum.

As can be seen from Fig. 5 and Table 1, both the maximum OPEF intensity ( $I_{\max}^{\text{OPEF}}$ ) and the  $\Phi$  of **CZ** increase upon increasing the solvent polarity, showing the negative solvatokinetic effect. For example, the  $\Phi$  of **CZ** in highly polar DMF is more than six times that in slightly polar toluene. This should be due to the proximity effect [31]. The vibronic coupling of the  $n-\pi^*$  state with the lowest  $\pi-\pi^*$  state increases non-radiative decay (internal conversion and / or intersystem crossing), which can be weakened in polar solvents. In contrast to **CZ**, the other target compounds (**PTZ**,

**CZ-Py1**, **CZ-Py2**, **CZ-BI1**, and **CZ-BI2**) show the positive solvatokinetic effect. With a rise in the solvent polarity, both the  $I_{\max}^{\text{OPEF}}$  and the  $\Phi$  decrease consistently and significantly. Especially, the  $\Phi$  values dramatically drop to 0.02 for **PTZ**, 0.01 for **CZ-Py1**, 0.005 for **CZ-Py2**, 0.02 for **CZ-BI1**, and 0.006 for **CZ-BI2** in highly polar DMF. This fluorescent behavior may be attributed to the formation of the twisted intramolecular charge transfer (TICT) state which is usually characterized by enhanced charge transfer accompanied by a twist of the bond joining the donor and the acceptor [32]. The polarity-dependent TICT state is non-emissive because of rapid intersystem crossing to non-radiative triplets.

#### 2.4. Two-photon properties

As a consequence of their relatively strong fluorescence, the TPA response of all the target compounds in the near infrared (NIR) region was experimentally determined by the well-known two-photon induced fluorescence method [33]. Their corresponding nonlinear photophysical properties in toluene and THF are listed in Table 3. The representative two-photon excited fluorescence (TPEF) spectra of **CZ-BI2** in THF are shown in Fig. S1. Under excitation of 690-930 nm femtosecond laser pulses, they all emit frequency up-converted fluorescence with the maximum TPEF wavelengths ( $\lambda_{\max}^{\text{TPEF}}$ ) at 471-561 nm (toluene) and 496-575 nm (THF). Compared with the  $\lambda_{\max}^{\text{OPEF}}$ , the  $\lambda_{\max}^{\text{TPEF}}$  values are obviously red-shifted owing to the reabsorption effect. Since the linear absorption spectra in the long wavelength sides and the OPEF spectra in the short wavelength sides overlap. Furthermore, concentrated solution ( $1 \times 10^{-3}$  mol L<sup>-1</sup>) instead of dilute solution ( $1 \times 10^{-6}$  mol L<sup>-1</sup>) was used in the TPEF measurement. The reabsorption of the short wavelength fluorescence can no longer be neglected. As shown in Fig. S1, it is obvious that the TPEF intensity is significantly associated with the excitation wavelengths, while the excitation wavelengths slightly affect the TPEF peak shapes and positions. All the target compounds exhibit a single TPEF peak. Considering the introduction of electron donors and acceptors which may produce the strong push-pull electronic

effect, this phenomenon indicates that the emitting state here should not be the locally excited (LE) state but the ICT state.

**Table 3**

Nonlinear photophysical properties of the target compounds.

| Compound      | Solvent | $\lambda_{\max}^{\text{TPEF}}$ <sup>a</sup><br>(nm) | $\sigma_{\max}$ <sup>b</sup><br>(GM) | $\sigma_{\max} / \text{MW}$ <sup>c</sup><br>(GM g <sup>-1</sup> mol) |
|---------------|---------|---|--------------------------------------|--|
| <b>PTZ</b>    | Toluene | 561   | 104                                  | 0.289 (0.8)  |
|               | THF     | 575   | 132                                  | 0.367 (0.7)  |
| <b>CZ</b>     | Toluene | 471   | 115                                  | 0.351 (1.0)  |
|               | THF     | 496   | 182                                  | 0.555 (1.0)  |
| <b>CZ-Py1</b> | Toluene | 511   | 328                                  | 0.566 (1.6)  |
|               | THF     | 520   | 453                                  | 0.782 (1.4)  |
| <b>CZ-Py2</b> | Toluene | 518   | 532                                  | 0.641 (1.8)  |
|               | THF     | 524   | 844                                  | 1.017 (1.8)  |
| <b>CZ-BI1</b> | Toluene | 521   | 787                                  | 1.245 (3.5)  |
|               | THF     | 529   | 1244                                 | 1.968 (3.5)  |
| <b>CZ-BI2</b> | Toluene | 525   | 1500                                 | 1.603 (4.6)  |
|               | THF     | 536   | 2072                                 | 2.214 (4.0)  |

<sup>a</sup> Maximum two-photon excited fluorescence wavelength,  $c = 1 \times 10^{-3} \text{ mol L}^{-1}$ .

<sup>b</sup> Maximum two-photon absorption cross-section,  $1 \text{ GM} = 1 \times 10^{-50} \text{ cm}^4 \text{ s photon}^{-1}$ .

<sup>c</sup> Maximum two-photon absorption cross-section divided by molecular weight. The numbers in the parentheses are the relative values.

It is observed from Fig. 2 that the target compounds are highly transparent above 500 nm, indicating that the laser wavelengths (690-930 nm) used in the TPEF measurement are out of the linear absorption region. The representative TPEF spectra of **CZ-BI2** in THF at 830 nm under different pump powers are shown in Fig. 8. The

inset displays the logarithmic plot of its fluorescence integral ( $I_{out}$ ) versus different pump powers ( $I_{in}$ ). The slope derived from the fitted line is 2.05. For the other target compounds, the relationship between fluorescence intensity and pump powers also follows the square law. These validate that the detected up-converted fluorescence emission really comes from the TPA process.

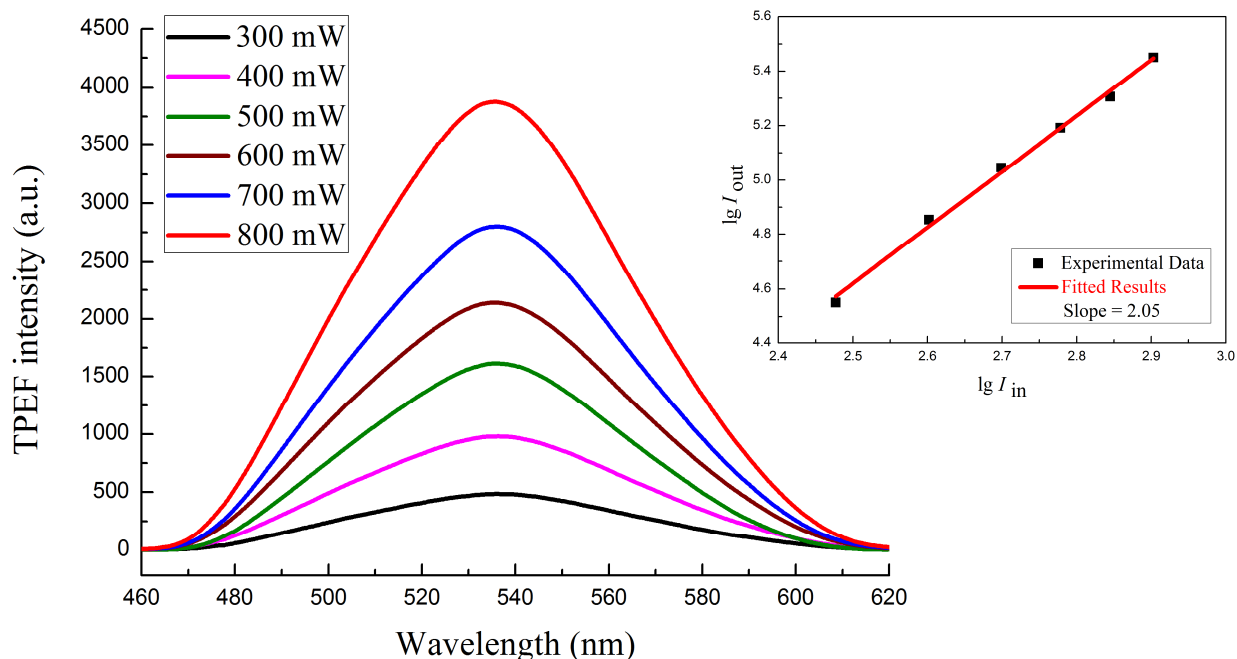


**Fig. 8.** Two-photon excited fluorescence spectra of **CZ-BI2** in THF ( $c = 1 \times 10^{-3}$  mol  $L^{-1}$ ) at 830 nm under different pump powers. The inset is the logarithmic plot of the fluorescence integral ( $I_{out}$ ) of **CZ-BI2** versus different pump powers ( $I_{in}$ ).

The  $\sigma$  values are obtained by comparing the TPEF intensity of the samples with that of a reference compound using the following Equation (3) [33]:

$$\sigma_s = \frac{F_s \Phi_r n_r c_r}{F_r \Phi_s n_s c_s} \sigma_r \quad (2)$$

where the subscripts s and r denote the sample and the reference, respectively.  $F$  and  $\Phi$  represent the TPEF integral intensity and the fluorescence quantum yield.  $n$  and  $c$  are the refractive index and the concentration of the solution. In this work, we selected

fluorescein in 0.1 mol L<sup>-1</sup> sodium hydroxide ( $c = 1 \times 10^{-3}$  mol L<sup>-1</sup>) as the reference. Its  $\sigma$  values at different excitation wavelengths had been determined by Webb *et al.* [33b].

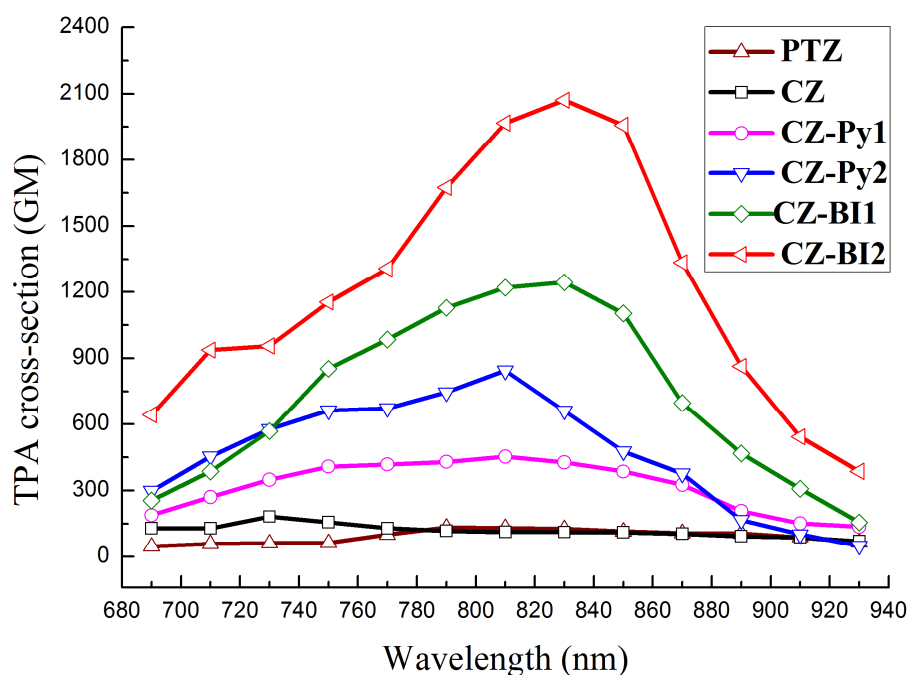


**Fig. 9.** Two-photon absorption cross-sections of the target compounds in THF under different excitation wavelengths.

Figs. 9 and S2 show the  $\sigma$  values of the target compounds in the 690-930 nm region. One can see that the optimal excitation wavelengths in both solvents (THF and toluene) are 730 (**CZ**), 790 (**PTZ**), 810 (**CZ-Py1**, **CZ-Py2**), and 830 (**CZ-BI1**, **CZ-BI2**) nm, respectively, which appear at about twice the wavelengths of the low-energy one-photon absorption bands. This phenomenon indicates that the absorption of the ICT state plays a dominant role. The  $\sigma$  values also display solvent polarity dependencies. As can be seen by comparing Fig. 9 with Fig. S2, the  $\sigma$  values obtained in moderately polar THF are larger than those obtained in slightly polar toluene, which may be due to the stronger solute-solvent interaction in THF. The  $\sigma$  maxima ( $\sigma_{\max}$ ) of the single-branched compounds **CZ** and **PTZ** in THF (toluene) are

182 (115) and 132 (104) GM, respectively. The small decrease from **CZ** to **PTZ** is ascribed to the nonplanar structure of the phenothiazine ring, which may impede electron transport. One can observe moderate or significant enhancement of the  $\sigma_{\max}$  for the double-branched compounds by factors of 2.5-2.9 (**CZ-Py1**) and 6.8 (**CZ-BI1**), relative to the single-branched compound (**CZ**). This can be attributed to the introduction of a quasi-quadrupolar A- $\pi$ -D- $\pi$ -A' branch different from the original dipolar D- $\pi$ -A branch, which not only elongates the conjugation pathway, but also modulates the push-pull electronic mode. As the number of branches is changed systematically from two to three by introducing another identical A- $\pi$ -D- $\pi$ -A' branch, the  $\sigma_{\max}$  values are found to increase almost additively. For example, the  $\sigma_{\max}$  of **CZ-BI2** rises by 713 (828) GM in toluene (THF) with respect to that of **CZ-BI1**, which is approximately the same as the increase in the  $\sigma_{\max}$  observed from **CZ** to **CZ-BI1** (672 GM in toluene and 1062 GM in THF). This fact reveals that the coupling between the branches is weak. For the series (**CZ**, **CZ-BI1**, and **CZ-BI2**), the  $\sigma_{\max}$  values rise in a proportion of 1.0 : 6.8 : 11.4-13.0, and the ratio of  $\sigma_{\max} / MW$ , which is defined as the  $\sigma_{\max}$  divided by the molecular weight, is 1.0 : 3.5 : 4.0-4.6. It is obvious that both the  $\sigma_{\max}$  (1.0 : 2.5-2.9 : 4.6) and the  $\sigma_{\max} / MW$  (1.0 : 1.4-1.6 : 1.8) of the series (**CZ**, **CZ-Py1**, and **CZ-Py2**) are greatly smaller. The significantly different TPA magnitude of the two series is closely related to the fact that the peripheral pyridine acceptor (**CZ-Py1**, **CZ-Py2**) is replaced with the benzimidazole acceptor (**CZ-BI1**, **CZ-BI2**). Compared with pyridine, benzimidazole has stronger electron-withdrawing ability, which can be proved from the  $^1\text{H}$  NMR spectra. The protons in the olefinic group linked directly to benzimidazole exhibit higher chemical shifts. Therefore, a reasonable explanation is that the benzimidazole acceptor is able to promote electron delocalization to a greater extent. At the microscopic level, the  $\sigma$  is related to the imaginary part of the molecular third-order nonlinear susceptibility (second-order hyperpolarizability,  $\gamma$ ). A simplified model expression for the  $\gamma$  is obtained from the Sum-Over-States (SOS) expression, which can be written as Equation (4) [34]:

$$\gamma_{xxxx[\text{model}]} = 24 \frac{M_{ge}^2 \Delta\mu_{ge}^2}{E_{ge}^3} - 24 \frac{M_{ge}^4}{E_{ge}^3} + 24 \sum_{e'} \frac{M_{ge}^2 M_{ee'}^2}{E_{ge}^2 E_{ge'}} \quad (4)$$

Where  $M_{ge}$ ,  $\Delta\mu_{ge}$ , and  $E_{ge}$  are the transition dipole moment, the difference in the dipole moments, and the transition energy between the ground state and the first excited state, respectively.  $M_{ee'}$  is the transition dipole moment between the first excited state and the two-photon allowed higher excited states.  $E_{ge'}$  is the transition energy between the ground state and the two-photon allowed higher excited states.

According to Equation (4), the  $\sigma$  can be enhanced by (1) decreasing the transition energy ( $E_{ge}$ ,  $E_{ge'}$ ), (2) increasing the difference in the dipole moments ( $\Delta\mu_{ge}$ ), and (3) increasing the transition dipole moment ( $M_{ge}$ ,  $M_{ee'}$ ). It can be seen from the linear absorption spectra and the TDDFT calculation results that the  $E_{ge}$  and the  $E_{ge'}$  decrease monotonically following the order: **CZ-BI2** < **CZ-BI1** < **CZ-Py2** < **CZ-Py1**. Based on the Lippert-Mataga equation, the  $\Delta\mu_{ge}$  deduced from the relationship between the  $\Delta\nu$  and the  $\Delta f$  can be sequenced as **CZ-BI1** > **CZ-Py1** and **CZ-BI2** > **CZ-Py2**. The square of the  $M_{ge}$  shows positive correlation with the  $\epsilon$  [35]. As seen in Table 1, an increase in the  $\epsilon$  values is evident when going from **CZ-Py1** (**CZ-Py2**) to **CZ-BI1** (**CZ-BI2**), indicating a change in the  $M_{ge}$  (**CZ-BI1** > **CZ-Py1** and **CZ-BI2** > **CZ-Py2**). All the above evidence further explains the observed experimental results, which is that the  $\sigma_{\max}$  values of **CZ-BI1** and **CZ-BI2** are much larger than those of **CZ-Py1** and **CZ-Py2**.

### 3. Conclusion

A series of novel asymmetric branched compounds that utilize a 1,3,5-triazine core and feature D- $\pi$ -A-( $\pi$ -D'- $\pi$ -A')<sub>0-2</sub> configurations were synthesized using the dehydration condensation reaction and fully characterized. Their linear and nonlinear

photophysical properties were studied in detail through the experiments and the TDDFT calculations. Some interesting structure-property relationships were also revealed. Our investigation shows that the target compounds do not exhibit the strong cooperative effect associated with the non-additive enhancement of  $\sigma$ . But based on the  $\sigma$  values of **CZ-BI1** and **CZ-BI2** (787-2072 GM), which are much larger than those of the analogous compounds **CZ-Py1** and **CZ-Py2** (328-844 GM), it is possible to infer that the benzimidazole acceptor can be a very useful TPA structural unit. We will further functionalize **CZ-BI1** and **CZ-BI2** by forming the benzimidazolium salts with the expectation that they will possess good water solubility combined with desirable one- and two-photon absorption and luminescence properties for the application in bioimaging.

## 4. Experimental section

### 4.1. Materials and instruments

The solvent DMF was pre-dried before use. The other materials were commercially available and were used without further purification.

Melting points were measured on an X-4 micromelting point apparatus without correction.  $^1\text{H}$  and  $^{13}\text{C}$  NMR spectra were collected on a Bruker AVANCE III 500 apparatus, with TMS as an internal standard and DMSO- $d_6$  as a solvent. FT-IR spectra were recorded on a Thermo Nicolet 6700 spectrometer using KBr pellets. Mass spectra were taken on a Thermo Scientific LTQ Orbitrap XL mass spectrometry instrument.

The linear absorption spectra were measured on a Shimadzu UV-2550 UV-visible spectrophotometer. The OPEF spectra measurements were performed using a RF-5301PC fluorescence spectrophotometer. The TPEF spectra were measured using a femtosecond Ti : Sapphire laser (Chameleon Ultra II) as the pump source with a pulse width of 140 fs and a repetition rate of 80 MHz, and tuned by step of 20 nm in the wavelength range of 690-930 nm.

## 4.2. Synthesis

### 4.2.1. 2,5-dimethoxy-4-[(1E)-2-(1-methyl-1H-benzimidazol-2-yl)ethenyl]benzaldehyde (**2c**)

A mixture of 1,2-dimethyl-1H-benzimidazole (1.46 g, 10 mmol), **2a** (1.94 g, 10 mmol), acetic anhydride (6 mL), and acetic acid (3 mL) was heated under reflux for 6 h, then cooled to room temperature. After concentrated hydrochloric acid (15 mL) was added, the mixture was filtered. The filtrate was neutralized with 30% aqueous sodium hydroxide solution (30 mL) and gave a precipitate. The precipitate was purified by column chromatography on silica gel using petroleum ether / ethyl acetate (8 : 1) as eluent to give yellow crystalline powder (2.26 g, 70.2%). m.p. 244-246 °C; <sup>1</sup>H NMR (DMSO-*d*<sub>6</sub>, 500 MHz)  $\delta$ : 10.36 (s, 1H), 8.17 (d, *J* = 16.0 Hz, 1H), 7.75 (s, 1H), 7.73 (d, *J* = 16.0 Hz, 1H), 7.64 (dd, *J*<sub>1</sub> = 6.9 Hz, *J*<sub>2</sub> = 1.3 Hz, 1H), 7.58 (dd, *J*<sub>1</sub> = 6.9 Hz, *J*<sub>2</sub> = 1.3 Hz, 1H), 7.31 (s, 1H), 7.22-7.28 (m, 2H), 4.03 (s, 3H), 3.99 (s, 3H), 3.92 (s, 3H); FT-IR (KBr)  $\nu$ : 3046, 2944, 2868, 1669, 1602, 1465, 1402, 1334, 1267, 1210, 1039, 973, 745, 602; HRMS (ESI): *m/z* calcd for C<sub>19</sub>H<sub>19</sub>N<sub>2</sub>O<sub>3</sub> [M+H]<sup>+</sup>: 323.1396; found: 323.1392.

### 4.2.2. 3-[(1E)-2-(4,6-dimethyl-1,3,5-triazin-2-yl)ethenyl]-9-ethyl-9H-carbazole (**CZ**)

To a mixture of **1a** (0.55 g, 4.5 mmol), potassium hydroxide (0.3 g), and methonal (30 mL) was added a solution of **4a** (0.67 g, 3 mmol) in methanol (30 mL) dropwise. The reaction mixture was refluxed for 20 h and then the solvent was removed. The residue was purified by column chromatography on silica gel using petroleum ether / ethyl acetate (10 : 1) as eluent to give bright yellow needle crystals (0.68 g, 69.1%). m.p. 156-157 °C; <sup>1</sup>H NMR (DMSO-*d*<sub>6</sub>, 500 MHz)  $\delta$ : 8.68 (d, *J* = 1.1 Hz, 1H), 8.35 (d, *J* = 15.9 Hz, 1H), 8.25 (d, *J* = 7.6 Hz, 1H), 7.93 (dd, *J*<sub>1</sub> = 8.6 Hz, *J*<sub>2</sub> = 1.1 Hz, 1H), 7.68 (d, *J* = 8.6 Hz, 1H), 7.66 (d, *J* = 8.2 Hz, 1H), 7.50 (t, *J* = 7.6 Hz, 1H), 7.27 (t, *J* = 7.6 Hz, 1H), 7.21 (d, *J* = 15.9 Hz, 1H), 4.49 (q, *J* = 7.1 Hz, 2H), 2.56 (s, 6H), 1.34 (t, *J* = 7.1 Hz, 3H); <sup>13</sup>C NMR (DMSO-*d*<sub>6</sub>, 125 MHz)  $\delta$ : 175.40, 170.76, 142.90, 140.72, 140.06, 126.26, 126.23, 125.88, 122.73, 122.27, 122.17, 121.38, 120.72, 119.42, 109.62, 109.50, 37.15, 25.21, 13.72; FT-IR (KBr)  $\nu$ : 3051, 2967, 2874, 1622, 1524, 1475, 1388, 1337, 1234, 976, 742; HRMS (ESI): *m/z* calcd for C<sub>21</sub>H<sub>21</sub>N<sub>4</sub> [M+H]<sup>+</sup>:

329.1766; found: 329.1758.

4.2.3. 3-[(1*E*)-2-(4,6-dimethyl-1,3,5-triazin-2-yl)ethenyl]-10-ethyl-10*H*-phenothiazine (**PTZ**)

This compound was synthesized using a procedure similar to that described for **CZ**, with **3a** instead of **4a**. Orange-yellow crystalline powder. Yield 63.8%. m.p. 85-87 °C; <sup>1</sup>H NMR (DMSO-*d*<sub>6</sub>, 500 MHz) δ: 8.02 (d, *J* = 15.9 Hz, 1H), 7.60 (dd, *J*<sub>1</sub> = 8.6 Hz, *J*<sub>2</sub> = 2.0 Hz, 1H), 7.57 (d, *J* = 2.0 Hz, 1H), 7.21 (td, *J*<sub>1</sub> = 7.7 Hz, *J*<sub>2</sub> = 1.5 Hz, 1H), 7.15 (dd, *J*<sub>1</sub> = 7.6 Hz, *J*<sub>2</sub> = 1.5 Hz, 1H), 7.04 (d, *J* = 7.7 Hz, 1H), 7.03 (d, *J* = 15.9 Hz, 1H), 7.02 (d, *J* = 8.6 Hz, 1H), 6.96 (td, *J*<sub>1</sub> = 7.6 Hz, *J*<sub>2</sub> = 0.7 Hz, 1H), 3.95 (q, *J* = 6.9 Hz, 2H), 2.53 (s, 6H), 1.32 (t, *J* = 6.9 Hz, 3H); <sup>13</sup>C NMR (DMSO-*d*<sub>6</sub>, 125 MHz) δ: 175.56, 170.51, 145.83, 143.37, 140.38, 129.22, 128.46, 127.86, 127.11, 126.43, 123.47, 123.13, 122.93, 122.09, 115.67, 115.41, 41.45, 25.22, 12.58; FT-IR (KBr) ν: 3053, 2920, 2850, 1631, 1530, 1464, 1391, 1328, 1246, 980, 761; HRMS (ESI): *m/z* calcd for C<sub>21</sub>H<sub>21</sub>N<sub>4</sub>S [M+H]<sup>+</sup>: 361.1487; found: 361.1479.

4.2.4. 3-[(1*E*)-2-[4-[(1*E*)-2-[2,5-dimethoxy-4-[(1*E*)-2-(4-pyridinyl)ethenyl]phenyl]ethenyl]-6-methyl-1,3,5-triazin-2-yl]ethenyl]-9-ethyl-9*H*-carbazole (**CZ-Py1**)

This compound was synthesized using a procedure similar to that described for **CZ**, with **CZ** instead of **1a** and **2b** instead of **4a**. Brick-red crystalline powder. Yield 45.7%. m.p. 168-170 °C; <sup>1</sup>H NMR (DMSO-*d*<sub>6</sub>, 500 MHz) δ: 8.71 (d, *J* = 1.1 Hz, 1H), 8.57 (d, *J* = 5.9 Hz, 2H), 8.49 (d, *J* = 16.1 Hz, 1H), 8.41 (d, *J* = 15.8 Hz, 1H), 8.28 (d, *J* = 7.7 Hz, 1H), 7.96 (dd, *J*<sub>1</sub> = 8.6 Hz, *J*<sub>2</sub> = 1.1 Hz, 1H), 7.71 (d, *J* = 16.6 Hz, 1H), 7.70 (d, *J* = 8.6 Hz, 1H), 7.67 (d, *J* = 8.2 Hz, 1H), 7.57 (d, *J* = 5.9 Hz, 2H), 7.54 (s, 1H), 7.51 (t, *J* = 7.6 Hz, 1H), 7.47 (s, 1H), 7.45 (d, *J* = 16.6 Hz, 1H), 7.37 (d, *J* = 16.1 Hz, 1H), 7.28 (t, *J* = 7.4 Hz, 1H), 7.26 (d, *J* = 15.8 Hz, 1H), 4.50 (q, *J* = 7.1 Hz, 2H), 4.00 (s, 3H), 3.97 (s, 3H), 2.63 (s, 3H), 1.35 (t, *J* = 7.1 Hz, 3H); <sup>13</sup>C NMR (DMSO-*d*<sub>6</sub>, 125 MHz) δ: 175.53, 171.03, 170.78, 152.26, 151.43, 149.80, 144.82, 142.86, 140.78, 140.12, 135.22, 127.79, 127.42, 127.24, 126.87, 126.33, 126.30, 125.98, 124.60, 122.81, 122.46, 122.32, 121.36, 120.98, 120.79, 119.47, 110.96, 110.13, 109.66, 109.54, 56.32, 56.27, 37.20, 25.48, 13.77; FT-IR (KBr) ν: 3047, 2923, 2851, 1623, 1594, 1519, 1371, 1346, 1234, 1211, 1041, 979, 859, 746, 615; HRMS (ESI): *m/z*

calcd for  $C_{37}H_{34}N_5O_2$   $[M+H]^+$ : 580.2713<sup>+</sup>; found: 580.2697.

4.2.4. 3-[(1*E*)-2-[4-[(1*E*)-2-[2,5-dimethoxy-4-[(1*E*)-2-(1-methyl-1*H*-benzimidazol-2-yl)ethenyl]phenyl]ethenyl]-6-methyl-1,3,5-triazin-2-yl]ethenyl]-9-ethyl-9*H*-carbazole (**CZ-BI1**)

This compound was synthesized using a procedure similar to that described for **CZ**, with **CZ** instead of **1a** and **2c** instead of **4a**. Orange-yellow crystalline powder. Yield 44.4%. m.p. 244-246 °C;  $^1H$  NMR (DMSO-*d*<sub>6</sub>, 500 MHz)  $\delta$ : 8.70 (d, *J* = 1.0 Hz, 1H), 8.50 (d, *J* = 16.1 Hz, 1H), 8.41 (d, *J* = 15.8 Hz, 1H), 8.28 (d, *J* = 7.7 Hz, 1H), 8.19 (d, *J* = 16.0 Hz, 1H), 7.95 (dd, *J*<sub>1</sub> = 8.6 Hz, *J*<sub>2</sub> = 1.0 Hz, 1H), 7.70 (d, *J* = 8.6 Hz, 1H), 7.66 (d, *J* = 8.2 Hz, 1H), 7.64 (dd, *J*<sub>1</sub> = 6.7 Hz, *J*<sub>2</sub> = 1.8 Hz, 1H), 7.63 (s, 1H), 7.62 (d, *J* = 16.0 Hz, 1H), 7.56 (dd, *J*<sub>1</sub> = 6.7 Hz, *J*<sub>2</sub> = 1.8 Hz, 1H), 7.55 (s, 1H), 7.51 (t, *J* = 7.6 Hz, 1H), 7.38 (d, *J* = 16.1 Hz, 1H), 7.28 (t, *J* = 7.4 Hz, 1H), 7.26 (d, *J* = 15.8 Hz, 1H), 7.21-7.27 (m, 2H), 4.49 (q, *J* = 7.1 Hz, 2H), 4.04 (s, 3H), 4.01 (s, 3H), 3.98 (s, 3H), 2.63 (s, 3H), 1.35 (t, *J* = 7.1 Hz, 3H);  $^{13}C$  NMR (DMSO-*d*<sub>6</sub>, 125 MHz)  $\delta$ : 175.49, 170.98, 170.74, 152.28, 151.59, 151.20, 142.89, 142.80, 140.73, 140.08, 136.10, 135.19, 129.70, 127.21, 126.83, 126.28, 126.25, 125.94, 124.83, 122.76, 122.44, 122.28, 122.11, 122.03, 121.31, 120.74, 119.41, 118.49, 115.46, 110.85, 110.11, 110.05, 109.61, 109.48, 56.42, 56.27, 37.15, 29.63, 25.43, 13.71; FT-IR (KBr)  $\nu$ : 3047, 2923, 2852, 1624, 1519, 1372, 1345, 1235, 1211, 1041, 974, 742; HRMS (ESI): *m/z* calcd for  $C_{40}H_{37}N_6O_2$   $[M+H]^+$ : 633.2978; found: 633.2968.

4.2.5. 3-[(1*E*)-2-[4,6-bis[(1*E*)-2-[2,5-dimethoxy-4-[(1*E*)-2-(4-pyridinyl)ethenyl]phenyl]ethenyl]-1,3,5-triazin-2-yl]ethenyl]-9-ethyl-9*H*-carbazole (**CZ-Py2**)

This compound was synthesized using a procedure similar to that described for **CZ** except that **1a** was replaced with **CZ** and **4a** was replaced with **2b**, the molar ratio between **2b** and **CZ** was changed from 1 : 1.5 to 3 : 1, and **CZ** was added to **2b** instead of the latter being added to the former. Brick-red crystalline powder. Yield 67.4%. m.p. 174-176 °C;  $^1H$  NMR (DMSO-*d*<sub>6</sub>, 500 MHz)  $\delta$ : 8.72 (d, *J* = 1.0 Hz, 1H), 8.57 (d, *J* = 6.1 Hz, 4H), 8.55 (d, *J* = 16.0 Hz, 2H), 8.46 (d, *J* = 15.8 Hz, 1H), 8.30 (d, *J* = 7.7 Hz, 1H), 7.97 (dd, *J*<sub>1</sub> = 8.7 Hz, *J*<sub>2</sub> = 1.0 Hz, 1H), 7.71 (d, *J* = 16.4 Hz, 2H), 7.70 (d, *J* = 8.7 Hz, 1H), 7.66 (d, *J* = 8.2 Hz, 1H), 7.56 (d, *J* = 6.1 Hz, 4H), 7.55 (s,

2H), 7.52 (t,  $J = 7.7$  Hz, 1H), 7.48 (s, 2H), 7.45 (d,  $J = 16.4$  Hz, 2H), 7.40 (d,  $J = 16.0$  Hz, 2H), 7.31 (d,  $J = 15.8$  Hz, 1H), 7.29 (t,  $J = 7.5$  Hz, 1H), 4.50 (q,  $J = 7.1$  Hz, 2H), 4.02 (s, 6H), 3.99 (s, 6H), 1.36 (t,  $J = 7.1$  Hz, 3H);  $^{13}\text{C}$  NMR (DMSO- $d_6$ , 125 MHz)  $\delta$ : 171.10, 170.91, 152.23, 151.38, 150.09, 144.49, 142.65, 140.74, 140.12, 135.06, 127.76, 127.42, 127.01, 126.35, 126.34, 126.28, 126.05, 124.63, 122.82, 122.78, 122.34, 121.25, 120.88, 120.80, 119.44, 110.78, 110.05, 109.59, 109.51, 56.28, 56.26, 37.19, 13.77; FT-IR (KBr)  $\nu$ : 3049, 2933, 2830, 1622, 1593, 1504, 1373, 1345, 1232, 1211, 1042, 976, 864, 747, 610; HRMS (ESI):  $m/z$  calcd for  $\text{C}_{53}\text{H}_{47}\text{N}_6\text{O}_4$   $[\text{M}+\text{H}]^+$ : 831.3659; found: 831.3646.

4.2.6. 3-[(1E)-2-[4,6-bis[(1E)-2-[2,5-dimethoxy-4-[(1E)-2-(1-methyl-1H-benzimidazol-2-yl)ethenyl]phenyl]ethenyl]-1,3,5-triazin-2-yl]ethenyl]-9-ethyl-9H-carbazole (**CZ-BI2**)

This compound was synthesized using a procedure similar to that described for **CZ** except that **1a** was replaced with **CZ** and **4a** was replaced with **2c**, the molar ratio between **2c** and **CZ** was changed from 1 : 1.5 to 3 : 1, and **CZ** was added to **2c** instead of the latter being added to the former. Orange-red crystalline powder. Yield 61.2%. m.p. 268-270 °C;  $^1\text{H}$  NMR (DMSO- $d_6$ , 500 MHz)  $\delta$ : 8.74 (d,  $J = 1.0$  Hz, 1H), 8.57 (d,  $J = 16.0$  Hz, 2H), 8.47 (d,  $J = 15.8$  Hz, 1H), 8.31 (d,  $J = 7.7$  Hz, 1H), 8.20 (d,  $J = 16.0$  Hz, 2H), 7.98 (dd,  $J_1 = 8.6$  Hz,  $J_2 = 1.0$  Hz, 1H), 7.71 (d,  $J = 8.6$  Hz, 1H), 7.67 (d,  $J = 8.2$  Hz, 1H), 7.65 (dd,  $J_1 = 6.7$  Hz,  $J_2 = 1.9$  Hz, 2H), 7.64 (s, 2H), 7.62 (d,  $J = 16.0$  Hz, 2H), 7.59 (s, 2H), 7.56 (dd,  $J_1 = 6.7$  Hz,  $J_2 = 1.9$  Hz, 2H), 7.52 (t,  $J = 7.6$  Hz, 1H), 7.43 (d,  $J = 16.0$  Hz, 2H), 7.32 (d,  $J = 15.8$  Hz, 1H), 7.29 (t,  $J = 7.4$  Hz, 1H), 7.22-7.28 (m, 4H), 4.50 (q,  $J = 7.1$  Hz, 2H), 4.07 (s, 6H), 4.03 (s, 6H), 3.98 (s, 6H), 1.36 (t,  $J = 7.1$  Hz, 3H);  $^{13}\text{C}$  NMR (DMSO- $d_6$ , 125 MHz)  $\delta$ : 171.10, 170.90, 152.28, 151.60, 151.20, 142.86, 142.68, 140.72, 140.08, 136.08, 135.09, 129.74, 127.19, 127.07, 126.36, 126.25, 126.02, 124.93, 122.79, 122.41, 122.30, 122.13, 122.04, 121.23, 120.78, 119.40, 118.46, 115.37, 110.77, 110.11, 110.05, 109.59, 109.48, 56.46, 56.26, 37.15, 29.61, 13.74; FT-IR (KBr)  $\nu$ : 3047, 2933, 2828, 1622, 1505, 1372, 1331, 1233, 1211, 1040, 973, 740; HRMS (ESI):  $m/z$  calcd for  $\text{C}_{59}\text{H}_{53}\text{N}_8\text{O}_4$   $[\text{M}+\text{H}]^+$ : 937.4190; found: 937.4184.

## Acknowledgements

We are grateful to the financial supports from the Natural Science Foundation of Zhejiang province, China (Grant Nos. LY19B060010 and LY15B030006) and the National Natural Science Foundation of China (Grant No. 21103151).

## References

- [1] Göppert-Mayer M. *Ann Phys* 1931; 9: 273-294.
- [2] (a) Lemercier G, Four M, Chevreux S. *Coord Chem Rev* 2018; 368: 1-12;  
(b) Lundén H, Glimsdal E, Lindgren M, Lopes C. *Opt Eng* 2018; 57: 030802-1-030802-13;  
(c) Price RS, Dubinina G, Wicks G, Drobizhev M, Rebane A, Schanze KS. *ACS Appl Mater Interfaces* 2015; 7: 10795-10805.
- [3] (a) Madhu A, Eraiah B, Manasa P, Basavapoornima C. *J Non-Cryst Solids* 2018; 495: 35-46;  
(b) Liu M, Quah HS, Wen SC, Li Y, Vittal JJ, Ji W. *J Phys Chem C* 2018; 122: 777-781;  
(c) Huang C, Wang KY, Yang ZJ, Jiang L, Liu RM, Su RL, Zhou ZK, Wang XH. *J Phys Chem C* 2017; 121: 10071-10077.
- [4] (a) Nemoto T, Kawakami R, Hibi T, Lijima K, Otomo K. *Microsc* 2015; 64: 9-15;  
(b) Feng RQ, Sun YM, Tian MG, Zhang G, Zhang RY, Guo LF, Li XC, Yu XQ, Zhao N. *J Mater Chem B* 2015; 3: 8644-8649;  
(c) Li S, Shen XQ, Li L, Yuan PY, Guan ZP, Yao SQ, Xu QH. *Langmuir* 2014; 30: 7623-7627.
- [5] (a) Li L, Wang P, Hu YL, Lin G, Wu YQ, Huang WH, Zhao QZ. *Spectrochim Acta Part A: Molec Biomolec Spectr* 2015; 139: 243-252;  
(b) Woods R, Feldbacher S, Zidar D, Langer G, Satzinger V, Schmidt V, Pucher N, Liska R, Kern W. *Opt Mater Express* 2014; 4: 486-498.
- [6] (a) Xiong Z, Zheng CL, Jin F, Wei RM, Zhao YY, Gao XZ, Xia YZ, Dong XZ,

- Zheng ML, Duan XM. *Sensor Actuator B: Chem* 2018; 274: 541-550;
- (b) Zandrini T, Taniguchi S, Maruo S. *Micromachines* 2017; 8: 35.
- [7] (a) Sun BB, Wang L, Li Q, He PP, Liu HL, Wang H, Yang Y, Li JB. *Biomacromolecules* 2017; 18: 3506-3513;
- (b) Shen XQ, Li S, Li L, Yao SQ, Xu QH. *Chem-Eur J* 2015; 21: 2214-2221.
- [8] Zhao YX, Li X, Wu FP, Fang XY. *J Photochem Photobiol A: Chem* 2006; 177:12-16.
- [9] He NN, Li B, Zhang H, Hua JL, Jiang SY. *Synthetic Met* 2012; 162: 217-224.
- [10] (a) Abbotto A, Beverina L, Bozio R, Facchetti A, Ferrante C, Pagani GA, Pedron D, Signorini R. *Chem Commun* 2003; 2144-2145;
- (b) Liu B, Hu X-L, Liu J, Zhao Y-D, Huang Z-L. *Tetrahedron Lett* 2007; 48: 5958-5962;
- (c) Kim HM, Cho BR. *Chem Commun* 2009; 153-164;
- (d) Zheng SJ, Leclercq A, Fu J, Beverina L, Padilha LA, Zojer E, Schmidt K, Barlow S, Luo JD, Jiang S-H, Jen AK-Y, Yi YP, Shuai ZG, Stryland EWV, Hagan DJ, Brédas J-L, Marder SR. *Chem Mater* 2007; 19: 432-442;
- (e) Li QQ, Huang J, Zhong AS, Zhong C, Peng M, Liu J, Pei ZG, Huang ZL, Qin JG, Li Z. *J Phys Chem B* 2011; 115: 4279-4285;
- (f) Hrobáriková V, Hrobárik P, Gajdoš P, Fitis I, Fakis M, Persephonis P, Zahradník P. *J Org Chem* 2010; 75: 3053-3068.
- [11] Wang YC, Jiang YH, Wang YZ, Wang GQ, Liu DJ, Hua JL. *Appl Phys A-Mater* 2017; 123: 516.
- [12] Yang J, Tan HQ, Li DY, Jiang T, Gao YT, Li B, Qu X, Hua JL. *RSC Adv* 2016; 6: 58434-58442.
- [13] Gu J, Wang YL, Chen W-Q, Dong X-Z, Duan X-M, Kawata S. *New J Chem* 2007; 31: 63-68.
- [14] Qiu XP, Lu R, Zhou HP, Zhang XF, Xu TH, Liu XL, Zhao YY. *Tetrahedron Lett* 2008; 49: 7446-7449.
- [15] (a) Zheng Y-C, Zheng M-L, Chen S, Zhao Z-S, Duan X-M. *J Mater Chem B* 2014; 2: 2301-2310;

- (b) Tian Y-P, Li L, Zhou Y-H, Wang P, Zhou H-P, Wu J-Y, Hu Z-J, Yang J-X, Kong L, Xu G-B, Tao X-T, Jiang M-H. *Cryst Growth Des* 2009; 9: 1499-1504;
- (c) Abbotto A, Beverina L, Bozio R, Facchetti A, Ferrante C, Pagani GA, Pedron D, Signorini R. *Org Lett* 2002; 4: 1495-1498;
- (d) Koo C-K, Wong K-L, Man CW-Y, Lam Y-W, So LK-Y, Tam H-L, Tsao S-W, Cheah K-W, Lau K-C, Yang Y-Y, Chen J-C, Lam MH-W. *Inorg Chem* 2009; 48: 872-878;
- (e) Kobayashi Y, Katayama T, Yamane T, Setoura K, Ito S, Miyasaka H, Abe J. *J Am Chem Soc* 2016; 138: 5930-5938;
- (f) Skonieczny K, Ciuciu AI, Nichols EM, Hugues V, Blanchard-Desce M, Flamigni L, Gryko DT. *J Mater Chem* 2012; 22: 20649-20664;
- (g) Zhang M, Li MY, Zhao Q, Li FY, Zhang DQ, Zhang JP, Yi T, Huang CH. *Tetrahedron Lett* 2007; 48: 2329-2333.
- [16] (a) Zhang X, Yu XQ, Yao JS, Jiang MH. *Synthetic Met* 2008; 158: 964-968;
- (b) Zhou WC, Guo HY, Lin JR, Yang FF. *J Iran Chem Soc* 2018; 15: 2559-2566;
- (c) Li FS, Zhao BD, Chen Y, Zhang YF, Wang T, Xue S. *Spectrochim Acta Part A: Molec Biomolec Spectr* 2017; 185: 20-26;
- (d) Yuan M-S, Wang Q, Wang W-J, Li T-B, Wang L, Deng W, Du Z-T, Wang J-R. *Dyes Pigments* 2012; 95: 236-243;
- (e) Lin T-C, Li M-L, Liu C-Y, Tsai M-Y, Lee Y-H, Febriani Y, Lin J-H, Shen Y-K. *Eur J Org Chem* 2014; 2014: 1615-1621.
- [17] (a) Cui YZ, Zhang Y, Zhou LL, Yu F. *Adv Mater Res* 2013; 652-654: 542-545;
- (b) Katan C, Charlot M, Mongin O, Droumaguet CL, Jouikov V, Terenziani F, Badaeva E, Tretiak S, Blanchard-Desce M. *J Phys Chem B* 2010; 114: 3152-3169;
- (c) Zhang LQ, Zou L, Xiao J, Zhou PC, Zhong C, Chen XG, Qin JG, Mariz IFA, Maçôas E. *J Mater Chem* 2012; 22: 16781-16790.
- [18] (a) Zhang F, Hu Q, Castañon A, He Y, Liu Y, Paul BT, Tuck CJ, Hague RJM, Wildman RD. *Addit Manuf* 2017; 16: 206-212;
- (b) Wang YC, Jiang YH, Liu DJ, Wang YZ, Wang GQ, Hua JL. *J Lumin* 2017; 190: 89-93;

- (c) Wang YC, Jiang YH, Wang YZ, Wang GQ, Liu DJ, Hua JL. *J Appl Phys* 2017; 122: 043101-1-043101-7;
- (d) Whitby R, Ben-Tal Y, Macmillan R, Janssens S, Raymond S, Clarke D, Jin J, Kay A, Simpson MC. *RSC Adv* 2017; 7: 13232-13239;
- (e) Gan XP, Wang Y, Ge XP, Li W, Zhang XZ, Zhu WJ, Zhou HP, Wu JY, Tian YP. *Dyes Pigments* 2015; 120: 65-73;
- (f) Huang S, Yang B-Z, Guo J-F, Ren A-M. *Mol Phys* 2014; 113: 584-607;
- (g) Gao YT, Qu Y, Jiang T, Zhang H, He NN, Li B, Wu JC, Hua JL. *J Mater Chem C* 2014; 2: 6353-6361.
- [19] (a) Fang Z, Samoc M, Webster RD, Samoc A, Lai Y-H. *Tetrahedron Lett* 2012; 53: 4885-4888;
- (b) Wang XM, Yang P, Xu GB, Jiang WL, Yang TS. *Synthetic Met* 2005; 155: 464-473;
- (c) Fang Z, Zhang XH, Lai YH, Liu B. *Chem Commun* 2009; 920-922;
- (d) Lin T-C, Lin W-L, Wang C-M, Fu C-W. *Eur J Org Chem* 2011; 2011: 912-921;
- (e) Gong L-J, Wang Y-H, Kang Z-H, Huang T-H, Lu R, Zhang H-Z. *Chin J Chem Phys* 2012; 25: 636-641;
- (f) Lin T-C, Chen Y-F, Hu C-L, Hsu C-S. *J Mater Chem* 2009; 19: 7075-7080.
- [20] (a) Daniel J, Mastrodonato C, Sourdon A, Clermont G, Vabre J-M, Goudeau B, Voltaire H, Arbault S, Mongin O, Blanchard-Desce M. *Chem Commun* 2015; 51: 15245-15248;
- (b) He TC, Lim ZB, Ma L, Li HR, Rajwar D, Ying YJ, Di ZY, Grimsdale AC, Sun HD. *Chem-Asian J* 2013; 8: 564-571;
- (c) Fakis M, Ftilis I, Stefanatos S, Vellis P, Mikroyannidis J, Giannetas V, Persephonis P. *Dyes Pigments* 2009; 81: 63-68.
- [21] Liu Z-Q, Fang Q, Cao D-X, Wang D, Xu G-B. *Org Lett* 2004; 6: 2933-2936.
- [22] Katan C, Terenziani F, Mongin O, Werts MHV, Porrès L, Pons T, Mertz J, Tretiak S, Blanchard-Desce M. *J Phys Chem A* 2005; 109: 3024-3037.
- [23] Schaefer FC, Peters GA. *J Org Chem* 1961; 26: 2778-2784.
- [24] Jin F, Cai Z-B, Huang J-Q, Li S-L, Tian Y-P. *J Mol Struct* 2015; 1093: 33-38.

- [25] Algul O, Duran N, Gulbol G. *Asian J Chem* 2007; 19: 3085-3092.
- [26] Venkatesan K, Satyanarayana VSV, Mohanapriya K, Khora SS, Sivakumar A. *Res Chem Intermed* 2015; 41:595-607.
- [27] Fei XN, Gu YC, Li C, Yang X. *J Fluoresc* 2012; 22: 807-814.
- [28] Reichardt C. *Chem Rev* 1994; 94: 2319-2358.
- [29] Lakowicz JR. *Principles of fluorescence spectroscopy*. 3rd ed. New York: Springer; 2006.
- [30] Demas JN, Crosby GA. *J Phys Chem* 1971; 75: 991-1024.
- [31] Shim SC, Kim MS. *J Chem Soc Perkin Trans* □ 1989; 1897-1901.
- [32] (a) Rettig W, Majenz W. *Chem Phys Lett* 1989; 154: 335-341;  
(b) Majumdar D, Sen R, Bhattacharyya K, Bhattacharyya SP. *J Phys Chem* 1991; 95: 4324-4329.
- [33] (a) Xu C, Webb WW. *J Opt Soc Am B* 1996;13: 481-491;  
(b) Alkota MA, Xu C, Webb WW. *Appl Optics* 1998; 37: 7352-7356.
- [34] (a) Meyers F, Marder SR, Pierce BM, Brédas JL. *J Am Chem Soc* 1994; 116: 10703-10714;  
(b) Kogej T, Beljonne D, Meyers F, Perry JW, Marder SR, Brédas JL. *Chem Phys Lett* 1998; 298: 1-6.
- [35] Paley MS, Harris JM, Looser H, Baumert JC, Bjorklund GC, Jundt D, Twieg RJ. *J Org Chem* 1989; 54: 3774-3778.

The research highlights are as follows:

1. A series of novel asymmetric branched compounds were synthesized and characterized.
2. The linear and nonlinear photophysical properties were systematically investigated.
3. The time-dependent density functional theory calculations were conducted to unravel their electronic structures.
4. The structure-property relationships were analyzed.

## **Author Statement**

Zhi-Bin Cai: Conceptualization, Validation, Formal analysis, Writing – Original,  
Draft, Writing - Review & Editing, Supervision

Li-Jun Chen: Investigation

Sheng-Li Li: Resources

Qing Ye: Investigation

Yu-Peng Tian: Resources

Journal Pre-proof

## **Conflicts of interest**

There are no conflicts of interest to declare.

Journal Pre-proof